Geoscientific
Model Development

Open Access

GNAQPMS-Hg v1.0, a global nested atmospheric mercury transport model: model description, evaluation and application to trans-boundary transport of Chinese anthropogenic emissions

H. S. Chen[1], **Z. F. Wang**[1], **J. Li**[1], **X. Tang**[1], **B. Z. Ge**[1], **X. L. Wu**[1], **O. Wild**[2], **and G. R. Carmichael**[3]

[1]LAPC, Institute of Atmospheric Physics, Chinese Academy of Sciences, Beijing, China
[2]Lancaster Environment Centre, Lancaster University, Lancaster, UK
[3]Center for Global and Regional Environmental Research (CGRER), University of Iowa, Iowa City, Iowa, USA

Correspondence to: Z. F. Wang (zifawang@mail.iap.ac.cn)

Abstract. Atmospheric mercury (Hg) is a toxic pollutant and can be transported over the whole globe due to its long lifetime in the atmosphere. For the purpose of assessing Hg hemispheric transport and better characterizing regional Hg pollution, a global nested atmospheric Hg transport model (GNAQPMS-Hg – Global Nested Air Quality Prediction Modeling System for Hg) has been developed. In GNAQPMS-Hg, the gas- and aqueous-phase Hg chemistry representing the transformation among three forms of Hg: elemental mercury (Hg(0)), divalent mercury (Hg(II)), and primary particulate mercury (Hg(P)) are calculated. A detailed description of the model, including mercury emissions, gas- and aqueous-phase chemistry, and dry and wet deposition is given in this study. Worldwide observations including extensive data in China have been collected for model evaluation. Comparison results show that the model reasonably simulates the global mercury budget and the spatiotemporal variation of surface mercury concentrations and deposition. Overall, model predictions of annual total gaseous mercury (TGM) and wet deposition agree with observations within a factor of 2, and within a factor of 5 for oxidized mercury and dry deposition. The model performs significantly better in North America and Europe than in East Asia. This can probably be attributed to the large uncertainties in emission inventories, coarse model resolution and to the inconsistency between the simulation and observation periods in East Asia. Compared to the global simulation, the nested simulation shows improved skill at capturing the high spatial variability of surface Hg concentrations and deposition over East Asia.

In particular, the root mean square error (RMSE) of simulated Hg wet deposition over East Asia is reduced by 24 % in the nested simulation. Model sensitivity studies indicate that Chinese primary anthropogenic emissions account for 30 and 62 % of surface mercury concentrations and deposition over China, respectively. Along the rim of the western Pacific, the contributions from Chinese sources are 11 and 15.2 % over the Korean Peninsula, 10.4 and 8.2 % over Southeast Asia, and 5.7 and 5.9 % over Japan. But for North America, Europe and western Asia, the contributions from China are all below 5 %.

1 Introduction

Since the Minamata event in Japan in the 1960s (Harada, 1995), the toxicity of mercury (Hg) on human health and the environment has caused widespread public concern. Hg is a persistent bio-accumulated pollutant, and the only heavy metal that can be transported globally in gaseous form (Schroeder and Munthe, 1998). As a result, Hg has been listed as a priority pollutant by many countries and international agencies. After a long struggle, the first global treaty (the Minamata Convention) aimed at reducing Hg emissions and releases was adopted and signed by 92 countries in 2013 (http://www.mercuryconvention.org/). This made an important advance towards joint action to control global Hg pollution and has brought higher requirements for understanding global Hg source–receptor relationships, especially the

impacts of high regional emissions (e.g., from China and India) on global Hg levels. However, besides the remaining uncertainties in emission estimates, poor understanding of the chemical transformation of atmospheric mercury has made assessment of long-range transport very challenging (AMAP/UNEP, 2013).

Atmospheric mercury models are powerful tools to assess the fate and transport of mercury in the atmosphere. A number of atmospheric mercury models have been developed to investigate the emissions, transport, chemistry, deposition and source–receptor relationships of Hg at global and regional scales. Global models include the GEOS-Chem model (Goddard Earth Observing System-Chemistry; Amos et al., 2012; Zhang et al., 2012), the CTM-Hg model (Chemistry Transport Model for Hg; Seigneur et al., 2004), the CAM-Chem-Hg model (Community Atmospheric Model with Chemistry for Hg; Lei et al., 2013), the ECHMERIT model (ECHAM5-MERcury-ITaly; De Simone et al., 2014), the MSCE-Hg-Hem model (Meteorological Synthesizing Centre-East Hemispheric Hg model; Travnikov and Ilyin, 2009), the DEHM model (Danish Eulerian Hemispheric Model; Christensen et al., 2004), and the GRAHM model (Global/Regional Atmospheric Heavy Metals; Dastoor and Durnford, 2014). Regional models include the CMAQ-Hg model (Community Multi-scale Air Quality model for Hg; Bash, 2010), the STEM-Hg model (Sulfur Transport and dEposition Model for Hg; Pan et al., 2008), the CAMx-Hg model (Comprehensive Air Quality Model with Extensions for Hg; ENVIRON, 2011) and the WRF-Chem-Hg model (Weather Research and Forecasting model with Chemistry for Hg; Gencarelli et al., 2014). Application of these models has greatly advanced our understanding of the global Hg cycle. However, several model intercomparison studies (Ryaboshapko et al., 2007; Bullock Jr. et al., 2008; Pirrone and Keating, 2010) have found that large uncertainties still exist in Hg models and there is much room for improvement, especially for simulation of reactive gaseous mercury (RGM) and dry deposition.

Mercury is released to the atmosphere from both anthropogenic and natural sources. Human activities have increased the amount of mercury cycling through the atmosphere–ocean–terrestrial system by about a factor of 3 (Selin, 2009), although anthropogenic sources are estimated to account for only 31 % of total Hg emissions (Pirrone et al., 2010). China has the world's largest Hg production, consumption and emissions and suffers the most serious Hg pollution (Jiang et al., 2006), but the impacts of its anthropogenic emissions on global Hg levels are still unclear. Previous modeling studies mainly focused on long-range transport of mercury from Asia. Based on the GEOS-Chem model, about 7–20 % of Hg deposition over the USA was found to originate from Asian anthropogenic sources, which was comparable to that from North American sources (Strode et al., 2008; Jaffe and Strode, 2008). Another modeling study using the CTM-Hg model with three emission scenarios indi-

cated that Asian anthropogenic emissions accounted for 14–25 % of Hg deposition over the USA (Seigneur et al., 2004). Travnikov (2005) reported a contribution to Hg deposition from total Asian sources (including both anthropogenic and natural emissions) of 15 % over Europe and 33 % over the Arctic. Corbitt et al. (2011) further pointed out that Asian emissions are the largest contributors to anthropogenic deposition to all ocean basins and these contributions are expected to further grow in the future. The above studies all treated Asian anthropogenic emissions as a whole, and the effects of anthropogenic emissions from the world's largest single emitter (China) have not been explicitly assessed before. In addition, due to lack of observational data, little model validation has been conducted over East Asia (especially China) in these studies and this leads to greater uncertainty in the conclusions. Fu et al. (2012) reviewed previous modeling studies and pointed out that current model simulations tend to underestimate total gaseous mercury (TGM) and total particulate mercury (TPM) concentrations but overestimate reactive gaseous mercury (RGM) concentrations in China. To improve Hg model skill in China, nested simulations with high horizontal resolution might be a good choice. Zhang et al. (2012) demonstrated that a nested-grid model can capture the variation of Hg wet deposition over North America better than a global model. In this study, an online nested Hg simulation with flexible horizontal resolution was developed and evaluated. Compared to the traditional multi-scale modeling approach (using a global model to provide initial and boundary conditions to a regional model) (Seigneur et al., 2001), the online nested method uses the same physical and chemical parameterizations in the global and nested domains, which could avoid uncertainties induced by different boundary conditions. Compared to the offline nested method used in the GEOS-Chem model (Zhang et al., 2012), the online nested method can provide boundary conditions with higher time resolution (10 or 5 min) from the global domain to the nested domain. Hence, the online nested simulation would potentially improve model performance at a regional scale.

Therefore, a comprehensive evaluation and improvement of Hg model performance in China is needed to effectively reduce the uncertainties in Hg trans-boundary transport, and a quantitative assessment of Chinese anthropogenic contributions to global Hg concentration and deposition levels is helpful to determine and fulfill the Hg emission reduction tasks under the Minamata Convention.

In this paper, we describe the development of a global nested atmospheric mercury transport model (GNAQPMS-Hg – Global Nested Air Quality Prediction Modeling System for Hg) incorporating the latest available physical and chemical processes essential to the mercury life cycle. The spatial and temporal variability of Hg concentrations and deposition are comprehensively evaluated against available worldwide observations, including extensive data from China. The impact of horizontal resolution ($1° × 1°$ in the global domain

versus $0.33° \times 0.33°$ in the nested domain) on model predictions over East Asia is examined. Finally, the trans-boundary transport of Chinese primary anthropogenic Hg emissions is quantified using the model.

2 Model description and setup

2.1 General description

The atmospheric physics and chemistry component of GNAQPMS-Hg, with the exception of the mercury module, is based on the Nested Air Quality Prediction Modeling System for Hg (NAQPMS) (Wang et al., 2006), developed at the Institute of Atmospheric Physics, Chinese Academy of Sciences. NAQPMS is a 3-D regional Eulerian model which has been rigorously evaluated and widely applied to simulate the chemical evolution and transport of ozone (Li et al., 2007; Tang et al., 2010), the distribution and evolution of aerosol and acid rain over East Asia (Wang et al., 2002; Li et al., 2011; Li et al., 2012) and to provide operational air quality forecasts in megacities such as Beijing, Shanghai and Guangzhou (Wang et al., 2010; Wu et al., 2012; Wang et al., 2009). GNAQPMS is the global version of NAQPMS and uses the same model framework and physical and chemical parameterization schemes.

As a multi-scale model, GNAQPMS can simulate the transportation and formation of primary and secondary pollutants from urban to global scales using an online nesting approach. It includes advection, diffusion and convection processes, gas/aqueous/aerosol chemistry, and modules for dry and wet deposition. The advection process is parameterized based on an accurate mass conservative, peak-preserving algorithm provided by Walcek and Aleksic (1998). The gas-phase chemical mechanism is the CBM-Z mechanism (Carbon Bond Mechanism version Z; Zaveri and Peters, 1999), including 133 reactions for 53 species. The dry deposition module uses the parameterization of Wesely (1989). The wet deposition and aqueous-phase chemistry module is constructed based on a revised version of the RADM mechanism (Regional Acid Deposition Model; Chang et al., 1987; Wang et al., 2002; Ge et al., 2014). A mercury module has been developed and coupled into the GNAQPMS model in this study, as described in Sects. 2.2–2.4. Hereafter, we call this new model GNAQPMS-Hg. Note that meteorology, emissions, deposition and chemistry are self-consistent between the global and nested domains.

2.2 Mercury chemistry

2.2.1 Basic mechanism

In GNAQPMS-Hg, three forms of mercury are explicitly treated: elemental mercury (Hg(0)), divalent mercury (Hg(II)), and primary particulate mercury (Hg(P)). Transformations between these three forms include the gas-phase ox-
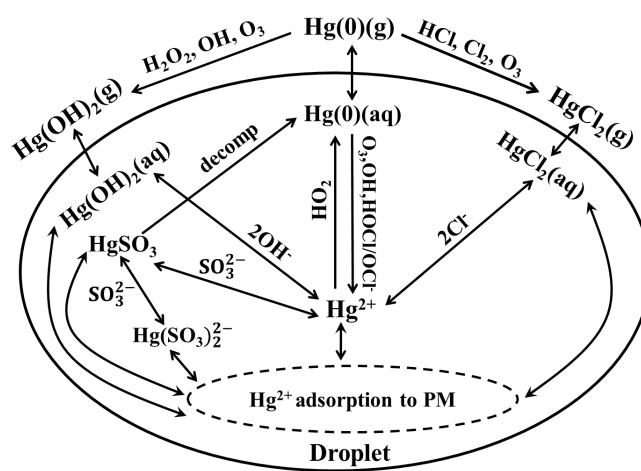

Figure 1. Schematic of different mercury reactions utilized in the GNAQPMS-Hg model.

idation of Hg(0) to Hg(II), the aqueous-phase oxidation of Hg(0) to Hg(II), the aqueous-phase reduction of Hg(II) to Hg(0), the aqueous-phase equilibria of Hg(II) species and the aqueous-phase adsorption of Hg(II) to PM. Figure 1 depicts the mercury reaction pathways both in the gas and aqueous phase while the detailed reactions and their rate constants are summarized in Table 1. In line with most global mercury models, GNAQPMS-Hg does not include dynamic air–surface exchange during mercury depletion events (MDEs) in polar regions (Schroeder et al., 1998) due to lack of fundamental data.

In the gas phase, Hg(0) is oxidized to Hg(II) by O_3, OH, hydrogen peroxide (H_2O_2), hydrogen chloride (HCl) and molecular chlorine (Cl_2). The oxidized products of these five reactions are assumed to be in the gas phase. According to Lin et al. (2004), OH and O_3 are the dominant oxidants in the continental troposphere while Cl and Br dominate Hg(0) oxidation in the marine boundary layer and the upper troposphere. In the aqueous phase, Hg(0) is oxidized to Hg(II) by dissolved O_3, OH, and Cl_2, and Hg(II) can be reduced back to Hg(0) via reaction with HO_2 and by the formation of sulfite complexes. In addition, adsorption of Hg(II) species on atmospheric particulate matter (PM) is simulated using an adsorption coefficient ($K = 34\,\text{L}\,\text{g}^{-1}$) recommended by Seigneur et al. (1998).

As shown in Table 1, the mercury chemistry requires the concentrations of several non-mercury species, among which O_3, OH, HO_2, H_2O_2, SO_2, HCl and PM are simulated online with GNAQPMS-Hg. However, Cl_2 is not explicitly simulated, and a typical vertical profile of Cl_2 concentrations is therefore prescribed. The Cl_2 concentrations are specified to be 100 ppt at the surface, 50 ppt aloft at night, 10 ppt during daytime over the oceans, and zero over land (Seigneur et al., 2001).

Table 1. Reactions and rate constants used in the GNAQPMS-Hg model.

No.	Reaction	Rates (k or K)*	References
Gas-phase reactions			
RG1	$Hg(0)(g)+O_3(g)\rightarrow Hg(II)(g)$	3×10^{-20} cm^3 molec^{-1} s^{-1}	Hall (1995)
RG2	$Hg(0)(g)+HCl(g)\rightarrow HgCl_2(g)$	1×10^{-19} cm^3 molec^{-1} s^{-1}	Hall and Bloom (1993)
RG3	$Hg(0)(g)+H_2O_2(g)\rightarrow Hg(OH)_2(g)$	8.5×10^{-19} cm^3 molec^{-1} s^{-1}	Tokos et al. (1998)
RG4	$Hg(0)(g)+Cl_2(g)\rightarrow HgCl_2(g)$	2.6×10^{-18} cm^3 molec^{-1} s^{-1}	Ariya et al. (2002)
RG5	$Hg(0)(g)+OH(g)\rightarrow Hg(OH)_2(g)$	8×10^{-14} cm^3 molec^{-1} s^{-1}	Sommar et al. (2001)
Gas–liquid equilibria			
GL1	$Hg(0)(g)\leftrightarrow Hg(0)(aq)$	0.11 M atm^{-1}	Sanemasa (1975)
GL2	$HgCl_2(g)\leftrightarrow HgCl_2(aq)$	1.4×10^6 M atm^{-1}	Lindqvist and Rodhe (1985)
GL3	$Hg(OH)_2(g)\leftrightarrow Hg(OH)_2(aq)$	1.2×10^4 M atm^{-1}	Lindqvist and Rodhe (1985)
Aqueous-phase equilibria			
AE1	$HgCl_2(aq)\leftrightarrow Hg^{2+}+2Cl^-$	1×10^{-14} M^2	Sillen et al. (1964)
AE2	$Hg(OH)_2(aq)\leftrightarrow Hg^{2+}+2OH^-$	1×10^{-22} M^2	Sillen et al. (1964)
AE3	$Hg^{2+} + SO_3^{2-} \leftrightarrow HgSO_3$	2.1×10^{13} M^{-1}	Van Loon et al. (2001)
AE4	$HgSO_3 + SO_3^{2-} \leftrightarrow Hg(SO_3)_2^{2-}$	1×10^{10} M^{-1}	Van Loon et al. (2001)
Aqueous-phase reaction			
RA1	$Hg(0)(aq)+O_3(aq)\rightarrow Hg^{2+}$	4.7×10^7 M^{-1} s^{-1}	Munthe (1992)
RA2	$Hg(0)(aq)+OH(aq)\rightarrow Hg^{2+}$	2×10^9 M^{-1} s^{-1}	Lin and Pehkonen (1997)
RA3	$HgSO_3(aq)\rightarrow Hg(0)(aq)$	0.0106 s^{-1}	Van Loon et al. (2000)
RA4	$Hg(II)(aq)+HO_2(aq)\rightarrow Hg(0)(aq)$	1.7×10^4 M^{-1} s^{-1}	Pehkonen and Lin (1998)
RA5	$Hg(0)(aq)+HOCl(aq)\rightarrow Hg^{2+}$	2.09×10^6 M^{-1} s^{-1}	Lin and Pehkonen (1998)
RA6	$Hg(0)(aq)+OCl^- \rightarrow Hg^{2+}$	1.99×10^6 M^{-1} s^{-1}	Lin and Pehkonen (1998)
Adsorption of Hg(II) on PM in the aqueous phase			
AD1	$Hg(II)(aq)\leftrightarrow Hg(II)(p)$	34 L g^{-1}	Seigneur et al. (1998)

* The reaction rate constants are for temperatures in the range of 20–25 °C. No temperature dependence information is available.

2.2.2 Bromine oxidation

In order to test the effect of bromine (Br) oxidation reactions on global Hg concentrations, five Br chemical reactions in the gas phase are added in addition to the O$_3$–OH oxidation mechanism. The detailed description of the Br chemical reactions and their implementation in the model is shown in Sect. S1.1 in the Supplement. A model sensitivity experiment with additional Br oxidation reactions was conducted and compared to the base case simulation with the O$_3$–OH oxidation mechanism. Figure S1 in the Supplement shows the difference of surface TGM concentrations resulting from introducing Br oxidation reactions. A decrease in TGM concentrations is found throughout the globe. This is because additional Br chemistry transforms more Hg(0) into Hg(II), which subsequently enhances the deposition of Hg(II), leading to the reduction of TGM concentrations. A larger TGM reduction is found in the Northern Hemisphere than in the Southern Hemisphere. In general, the change in TGM concentration is less than 0.2 ng m^{-3} in most areas, which indi-

cates that introducing Br chemistry seems to have little impact on overall TGM magnitudes and patterns. These results are similar to those of Lei et al. (2013) which test the impact of Br chemistry using the CAM-Chem-Hg model. Although adding the Br chemistry does not significantly change the TGM pattern, it may affect the gaseous Hg partitioning between Hg(0) and Hg(II) and hence may affect the global Hg deposition patterns. More in-depth tests and analyses are needed to address these impacts in the future. In the following sections, we still use the base case simulated results without considering the possible effects of Br chemistry.

2.2.3 Gas-particle partitioning of Hg(II)

Recent studies suggested that gas-particle partitioning of Hg(II) is an important process affecting global Hg concentrations and deposition (Amos et al., 2012). To test these effects, an empirical mechanism of gas-particle partitioning of Hg(II) was added to the GNAQPMS-Hg model. The detailed description of this mechanism and its implementation

in the model is shown in Sect. S1.2 in the Supplement. A model sensitivity experiment with a Hg(II) gas-particle partitioning module was conducted and compared to the base case simulation with all Hg(II) existing in the gas phase. Figures S2–S3 in the Supplement show the change fraction of surface TGM concentrations and oxidized Hg concentrations resulting from introducing the Hg(II) gas-particle partitioning mechanism. As expected, TGM concentrations decrease while oxidized Hg concentrations increase in the whole globe. The change fractions of TGM and oxidized Hg concentrations are smaller than 0.1 over the middle latitude of the Northern Hemisphere and even smaller than 0.05 over China. Considering that the base case simulation has overestimated oxidized Hg concentrations in most areas, introducing the mechanism of gas-particle partitioning of Hg(II) would further increase this model discrepancy. Therefore, we still use the base case simulated results without considering the possible effects of gas-particle partitioning of Hg(II) in the following sections.

2.3 Mercury deposition

Deposition is the leading removal process of atmospheric mercury and also a major cause of mercury contamination in soil and water. Studies have shown that both dry and wet removal pathways are equally significant for the total deposition of mercury (Pirrone and Keating, 2010; Lin et al., 2006).

Dry deposition of Hg(0), Hg(II) and Hg(P) is accounted for in the GNAQPMS-Hg model and simulated with the Wesely (1989) resistance model, which considers the effect of different land cover types and characterizes the diurnal variation of dry deposition velocities. Henry's law constant for Hg(0) is set to $0.11\,\mathrm{M\,atm^{-1}}$ (Lin and Pehkonen, 1999) with a temperature factor of $-4970\,\mathrm{K}$ (Clever et al., 1985), and the surface reactivity is set to zero. Hg(II) represents $HgCl_2$ and $Hg(OH)_2$. Henry's law constant is assumed to be the same as HNO_3 because they have similar solubility (Bullock and Brehme, 2002). Like HNO_3, Hg(II) has a strong tendency to stick to surfaces and its dry deposition occurs readily, so the surface resistance for Hg(II) in the dry deposition scheme is set to zero. The Hg(P) dry deposition velocity is set equal to that for sulfate, similar to that applied in the CMAQ-Hg and STEM-Hg models (Bullock and Brehme, 2002; Pan et al., 2008). A more detailed description of the dry deposition scheme used in the model is given in Sect. S2.1 in the Supplement. Model intercomparison studies demonstrate that there are still very large uncertainties in Hg dry deposition estimates (Bullock et al., 2008), and this can be ascribed to the wide range of treatments and physical parameters for dry deposition used in different models.

The wet deposition of Hg includes in-cloud and below-cloud scavenging. In-cloud scavenging is dependent on cloud and rain water content, species solubility and chemical transformation in the liquid phase, while below-cloud scavenging depends mainly on total rainfall intensity and washout effi-

ciency. Among the three forms of mercury, wet deposition of Hg(0) is minor compared to Hg(II) and Hg(P) due to its low solubility. Therefore, Hg(0) oxidation will enhance total Hg wet deposition. In the GNAQPMS-Hg model, wet deposition of Hg species is calculated through adapting the RADM mechanism. The physical properties (e.g., Henry's law constant, surface reactivity, molecular diffusivity) used are the same as those in the dry deposition module. A more detailed description of the wet deposition scheme used in the model is given in Sect. S2.2 in the Supplement. Currently, the uncertainties of Hg wet deposition simulation are mainly from the assumptions made in the cloud scavenging process and the uncertainty associated with the precipitation fields (Seigneur et al., 2001; Lin et al., 2006).

2.4 Mercury emissions

We include anthropogenic emissions, biomass burning emissions, geogenic emissions, land re-emission and ocean emissions (including re-emission) of Hg in the model. Emissions from artisanal mining and volcanoes are neglected due to lack of fundamental data. The former is estimated to be $400\,\mathrm{Mg\,yr^{-1}}$ and the latter $90\,\mathrm{Mg\,yr^{-1}}$, and they account for about 5 and 1 % of global total Hg emissions (Pirrone et al., 2010). Note that biomass burning emissions, geogenic emissions, land and ocean emissions are all treated as Hg(0). Global Hg emissions in the model are compared to previous studies in Table 2, and their spatial distributions are given in Figs. S4–S6 in the Supplement.

Anthropogenic emissions in 2000 are derived from the Arctic Monitoring and Assessment Programme (AMAP) inventory (Pacyna et al., 2006; Wilson et al., 2006). This inventory has a horizontal resolution of $0.5° \times 0.5°$ and no seasonal variation. Following Selin et al. (2008), we increase the Asian (0–60° N, 65–150° E) Hg(0) emissions in the AMAP inventory by 50 % (about $300\,\mathrm{Mg\,yr^{-1}}$) to account for the regional underestimation identified by Jaffe et al. (2005). The modified inventory has a total emission of $2488\,\mathrm{Mg\,yr^{-1}}$, with Hg(0), Hg(II) and Hg(P) accounting for 63, 29 and 8 %, respectively. The major source regions are Asia and Africa, accounting for 59 % ($1480\,\mathrm{Mg\,yr^{-1}}$) and 16 % ($399\,\mathrm{Mg\,yr^{-1}}$), while Europe and North America contribute only 7 and 6 %. China has the largest emissions at country level (about $785\,\mathrm{Mg\,yr^{-1}}$), contributing 53 % and 32 % to the Asian and global anthropogenic Hg emissions, respectively. It is noted that the emissions over South Africa in this inventory were reported to be flawed (AMAP/UNEP, 2008) and much higher than reality. The effects of these flawed emissions on the simulated results are assessed in Section S3 in the Supplement.

Biomass burning emissions are specified by mapping an annual mean value of $675\,\mathrm{Mg\,yr^{-1}}$ (Friedli et al., 2009) to the spatial and temporal distribution of CO biomass burning emissions from the IPCC-AR5 (Intergovernmental Panel on Climate Change Fifth Assessment Report) emissions inven-

Table 2. Global budgets of TGM in the literature (in Mg yr^{-1}).

	Bergan et al. (1999)	Shia et al. (1999)	Lamborg et al. (2002)	Mason et al. (2002)	Seigneur et al. (2004)	Selin et al. (2007)	Selin et al. (2008)	This work
Total Sources	6050	6100	4400	6600	6411	7000	11 200	10 163
Anthropogenic	2150	2100	2600	2400	2143	2200	3400	2488
Land	2500	2000	1000	1600	2290	2000	2800	2675
Ocean	1400	2000	800	2600	1978	2800	5000	5000
Total Sinks	6050	6100	4200	6600	6411	7000	11 200	10 163
Wet deposition		2800		3920		2100		2283
Dry deposition		3300		2680		4700		7880
TGM Burden	6050	10 400	5220	5000	7690	5360	5600	5507
TGM lifetime (yr)	1	1.7	1.3	0.76	1.2	0.79	0.5	0.54

tory (Lamarque et al., 2010). The regional and monthly emission amounts are prescribed based on Friedli et al. (2009). A similar method has been used by Jung et al. (2009).

The geogenic emissions here represent mobilization of Hg by degassing from geological reservoirs. Following Selin et al. (2007), we consider a geogenic source of 500 Mg yr^{-1} distributed according to the locations of Hg mines (Frank, 1999) as an indicator of Hg deposits. No temporal variation is applied to the geogenic emissions.

Land and ocean emissions are not dynamically calculated in the model due to the large uncertainties associated with current parameterizations. Consistent with several previous studies (Selin et al., 2007; Seigneur et al., 2001), the global annual land re-emission of Hg is assumed to be 1500 Mg yr^{-1}. The biogenic CO emissions from the Global Emission InitiAtive (GEIA) inventory (Guenther et al., 2006) are used as spatial and temporal surrogates to map the land re-emission. Regional emission totals from different latitude zones and land uses are prescribed based on Mason (2009).

Ocean emissions in our model are specified as 5000 Mg yr^{-1} (including re-emission), close to the estimates of Selin et al. (2008). Similarly, ocean emissions are mapped according to the distribution of ocean biogenic CO emissions from the Precursors of Ozone and their Effects in the Troposphere (POET) inventory (Granier et al., 2005). Additionally, ocean emissions are adjusted to reflect several distribution characteristics: (1) ocean emissions are high in summer but low in winter (Strode et al., 2007), (2) ocean emissions are largest in the tropics and downwind of industrial regions (Strode et al., 2007; Soerensen et al., 2010b), and (3) ocean emissions are large at mid and high latitudes in the Southern Hemisphere due to high wind speeds (Selin et al., 2008).

2.5 Model setup

Two nested domains covering the whole globe and East Asia are configured in this study. The horizontal resolutions are 1° × 1° and 0.33° × 0.33°, respectively. Vertically, the model uses 20 terrain-following layers from the sur-

face to 20 km a.s.l., with a decreasing resolution with height. Roughly, the lowest 14–18 layers are in the troposphere and the remaining layers are in the stratosphere. The time step in the model calculation is 600 s. The input/output frequency is 6 h in the global domain but 3 h in the nested domain. The meteorological fields are provided by the global version of the Weather Research and Forecasting (WRF) model. The atmospheric lifetime of Hg(0) is 0.5–2 years (Schroeder and Munthe, 1998), so to ensure mixing through the global troposphere and approach steady state we conduct the simulation for a 4-year period, with the first 3 years used for initialization and the last year (2001) used for analyses.

Emissions of reactive gases and aerosols used in this study are from several databases: (1) the IPCC-AR5 anthropogenic and biomass burning emissions for 2000 (Lamarque et al., 2010); (2) the GEIA biogenic emissions for 2000 (Guenther et al., 2006) and lightning emissions of nitric oxide (NO$_x$) for 1983–1990 (Price et al., 1997); (3) the POET ocean emissions of volatile organic compounds (VOCs) for 2000 (Granier et al., 2005); and (4) the soil NO$_x$ emissions for 2001 from Yan et al. (2005). All emissions are interpolated and remapped to match the model grids of the global and nested domains. The initial and top boundary conditions for O$_3$, NO$_x$, and CO are taken from a global chemical transport model (MOZART-V2.4) with 2.8° resolution (Horowitz et al., 2003).

Two model simulations, with and without Chinese primary anthropogenic Hg emissions, are carried out in this study. The differences between the two simulations are attributed to the influence of Chinese primary anthropogenic Hg emissions.

3 Model evaluation

3.1 Observational data

Compared to reactive gases and aerosols, atmospheric Hg measurements are still quite sparse. Routine monitoring networks for atmospheric Hg concentrations and deposition

have only been established in Europe and North America. Lack of Hg observational data is a great restriction against advancing our understanding of global Hg cycling and improving our skill in modeling. There is an urgent need to establish a coordinated global Hg monitoring network for current Hg study (Sprovieri et al., 2010; Keeler et al., 2009).

The observational data set in this study is based partly on the database shared by the GEOS-Chem Hg modeling group (public access at https://github.com/GC-Hg/HgBenchmark; Selin et al., 2007, 2008; Holmes et al., 2010). This is supplemented with scattered Hg observations across East Asia collected from the literature. The observations used in this study are summarized as follows: (1) long-term TGM/GEM (gaseous elemental mercury) measurements at 51 land sites, with 49 in the Northern Hemisphere and 2 in the Southern Hemisphere; (2) long-term RGM/TPM measurements at 26 land sites, all in the Northern Hemisphere; (3) short-term Hg species measurements from six ship cruises; (4) wet deposition measurements from the MDN (the Mercury Deposition Network in North America, http://nadp.sws.uiuc. edu/nadpdata/mdnalldata.asp) and EMEP (the European Monitoring and Evaluation Programme, http://www.nilu.no/ projects/ccc/emepdata.html) monitoring networks, with 51 and 8 sites, respectively; (5) dry and wet deposition measurements at 19 sites in East Asia. Further information about the measurement sites and data sources is given in Tables S2–S5 in the Supplement. It should be noted that the time periods of the measurements do not all match with those of the simulation, and this difference may partially explain any model–observation discrepancies. The influence of the mismatch of time periods when comparing the simulated results with the observations was qualitatively analyzed and shown in Sect. S4.1 in the Supplement.

3.2 Global mercury budget

Figure 2 gives the global mercury budget in GNAQPMS-Hg, including the cycling among atmosphere, ocean and land. The total atmospheric burden of Hg is 5546 Mg, with Hg(0), Hg(II), and Hg(P) contributing 90, 9 and 1 %, respectively. Therefore, mercury in the atmosphere exists mainly as Hg(0). Total emissions and deposition of Hg are 5163 and 2866 Mg yr^{-1} over land (a net source), and 5000 and 7297 Mg yr^{-1} over ocean (a net sink), indicating that Hg is transported from land to ocean. For total deposition of Hg species, Hg(0) and Hg(II) / Hg(P) account for 38 and 62 % over Earth's surface. Over land, deposition of Hg(II) / Hg(P) is more prominent than that of Hg(0), while they are both important over the ocean. Our results for total Hg deposition over ocean and Hg(II) / Hg(P) deposition over land are very close to that of GEOS-Chem (Selin et al., 2008). However, Hg(0) deposition over land derived from GNAQPMS-Hg is much smaller. This may be due to the lower reactivity coefficient used in the dry deposition module in GNAQPMS-Hg
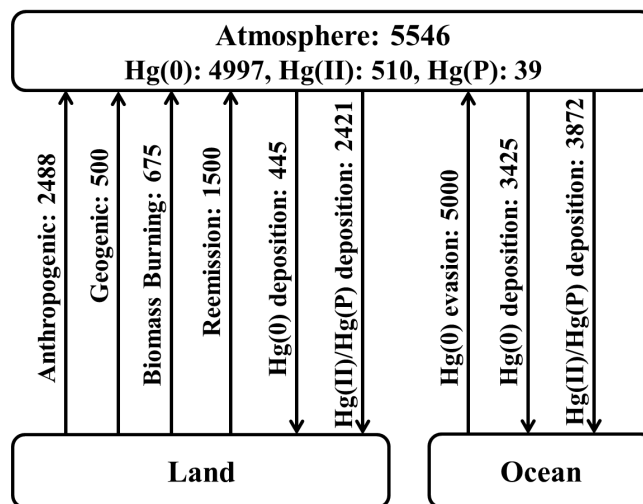

Figure 2. Global atmospheric mercury budget in GNAQPMS-Hg (in Mg yr^{-1}).

(zero in GNAQPMS-Hg but 10^{-5} in GEOS-Chem), which produces a lower dry deposition velocity for Hg(0).

Table 2 compares the GNAQPMS-Hg TGM budget and lifetime to those from previous modeling studies. The TGM sources, sinks, burden and lifetime estimated from GNAQPMS-Hg are all in the range determined by previous studies. Taking the TGM lifetime as an example, the reported range is 0.5–1.7 years and it is 0.54 years for GNAPQMS-Hg. In addition, similar to the results of GEOS-Chem (Selin et al., 2007) and CAM-Chem-Hg (Lei et al., 2013), Hg dry deposition in GNAQPMS-Hg dominates globally over wet deposition. Dry and wet deposition account for 78 and 22 %, respectively.

3.3 Total gaseous mercury (TGM)

As shown in Fig. 3, the main characteristics of the spatial distribution of TGM are captured well by the model. High surface TGM concentrations are found in or downwind of areas with intensive mercury-related mining (e.g., western USA) and rapid industrialization (e.g., East Asia). In particular, TGM concentrations even exceed 3 ng m^{-3} in eastern China. Both model simulations and observations show a significant surface interhemispheric gradient in TGM (Figs. 3, 4). Based on background observations, Lindberg et al. (2007) reported that mean Hg(0) concentrations were 1.5–1.7 ng m^{-3} in the Northern Hemisphere and 1.1–1.7 ng m^{-3} in the Southern Hemisphere. Lamborg et al. (2002) also estimated the range of north–south interhemispheric TGM concentration ratios for surface air as 1.2–1.8. Our model results share a general similarity with these studies. In GNAQPMS-Hg, surface mean TGM concentrations in the Northern Hemisphere and Southern Hemisphere are 1.56 and 1.23 ng m^{-3}, and the derived interhemispheric ratio is 1.27. However, it should
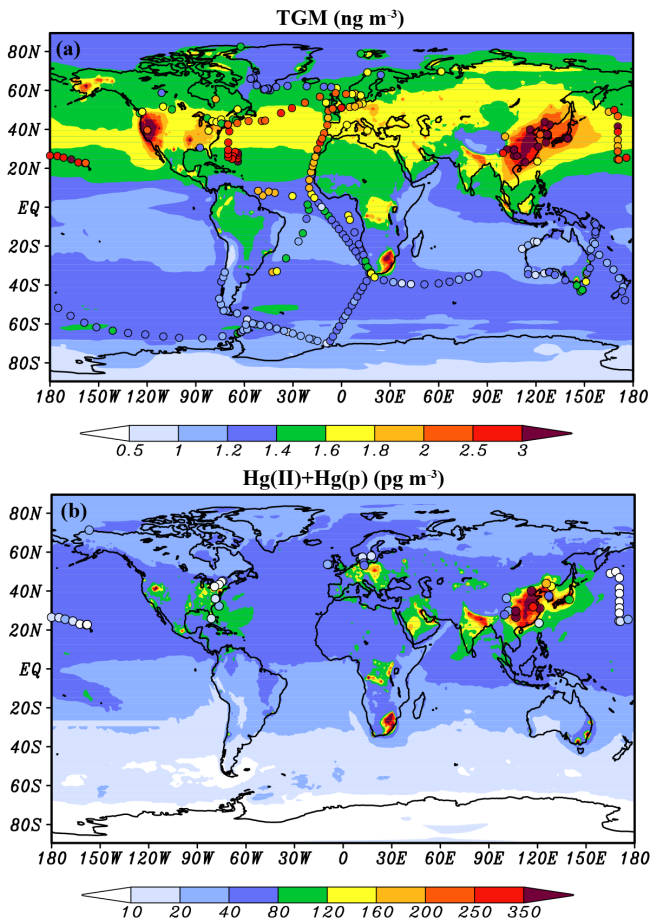
Figure 3. Annual average TGM **(a)** and oxidized mercury Hg(II)+Hg(P) **(b)** concentrations in surface air. Model results (background, for year 2001) are compared to observations (circles) from long-term surface sites and short-term ship cruises. Units of TGM and oxidized mercury are nanograms per cubic meter (ng m^{-3}) and picograms per cubic meter (pg m^{-3}), respectively.
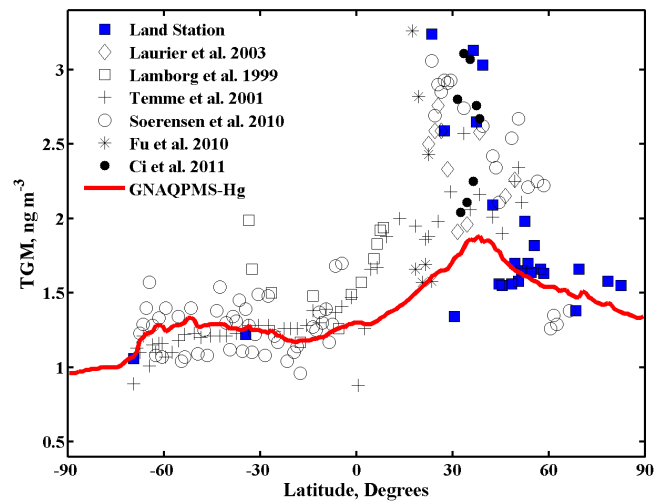

Figure 4. Variation of surface TGM concentrations (ng m^{-3}) with latitude. Zonally averaged, annual mean model results (line) are compared to observations (symbols).

be noted that GNAQPMS-Hg is systematically biased low relative to cruise observations in the Northern Hemisphere, which leads to underestimation of the TGM interhemispheric ratio compared with the range (1.49 ± 0.12) reported by Temme et al. (2003) based on observations from several Atlantic cruises. This disagreement was also found by several previous modeling studies (Seigneur et al., 2004; Selin et al., 2007) and can be attributed to the inability of current models to reproduce the air–sea exchange of Hg reasonably (Soerensen et al., 2010a). More specifically, this discrepancy is due to upwelling mercury from the subsurface ocean, possibly reflecting the legacy of past anthropogenic emissions (Holmes et al., 2010), and has been partially demonstrated by Soerensen et al. (2012). In general, the simulated TGM concentrations match observations within a factor of 2 (Fig. 10). The correlation coefficient (R) and normalized mean bias (NMB) between model results and observations from 51 land sites are 0.7 and -18 %, respectively (Table 3).

Figure 5 illustrates the mean seasonal variations of surface TGM concentrations in North America, Europe, East Asia, the Arctic, the Antarctic (Neumayer) and South Africa (Cape Point). In northern midlatitudes, TGM concentrations are high in winter but low in summer. This seasonality can be reproduced well by GNAQPMS-Hg. The summer low is caused by high OH concentrations and frequent precipitation (Bergan and Rodhe, 2001). Compared with observations, the simulated TGM monthly variations are stronger in North America but weaker in East Asia. The site by site comparisons in East Asia are shown in Fig. S9 in the Supplement. We can see that the nested simulation can improve model performance well for simulating TGM monthly variations in East Asia. At Arctic and Antarctic sites, TGM shows a spring minimum driven by MDEs and a summer maximum driven by re-emission from the snowpack (Steffen et al., 2005). The summer maximum is captured by GNAQPMS-Hg because high re-emission in polar summer has been taken into account in our land re-emission inventories. However, due to missing halogen chemistry, the model fails to reproduce the spring minimum. At Cape Point, both observed and simulated TGM show little seasonal variation. However, simulated monthly TGM concentrations are systematically biased high (NMB is 87 %), which can be attributed to the flawed anthropogenic emissions in the AMAP emission inventories over South Africa (AMAP/UNEP, 2008). By updating the anthropogenic emissions over South Africa, the simulated TGM concentrations at Cape Point decrease from 1.77 to 1.23 ng m^{-3}, more close to the observed values (See Sect. S3 in the Supplement).

An additional evaluation and analyses of simulated diurnal and vertical variation of TGM concentrations are given in Sect. S4.2 in the Supplement.
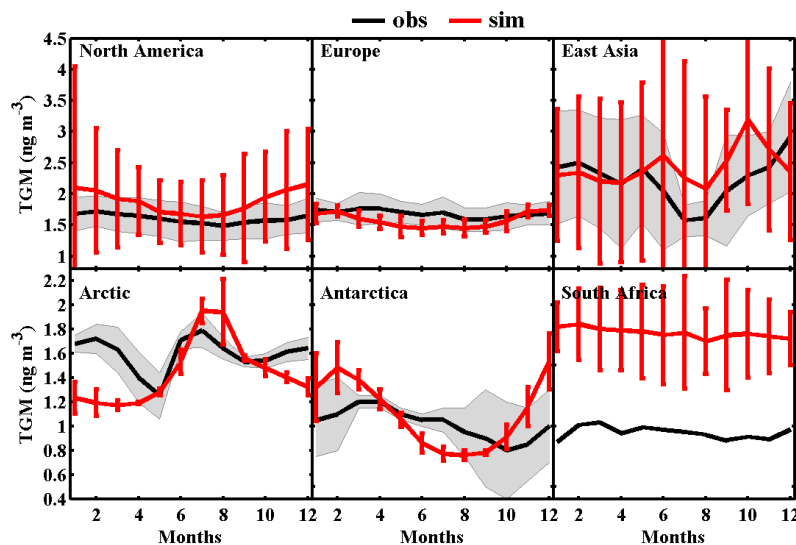
Figure 5. Mean seasonal variation of TGM (ng m^{-3}) over North America, Europe, East Asia, the Arctic, Antarctica and South Africa sites. Gray shaded areas and red vertical bars show 1 standard deviation over the sites for observations and for model results.

3.4 Oxidized mercury

Figure 3 also shows the global distribution of oxidized mercury (defined as the sum of RGM+TPM in the observations and Hg(II)+Hg(P) in the model). Similar to TGM, a pronounced north–south interhemispheric gradient is found for surface concentrations of oxidized mercury, which is consistent with the global distribution of emissions. Both the model simulation and observations indicate that oxidized mercury concentrations are much higher in East Asia than North America and Europe. Compared to scarce available observations, oxidized mercury concentrations are overestimated by GNAQPMS-Hg in most parts of the world (except East Asia). This discrepancy may partially be attributed to excessive oxidation of Hg(0) by relatively high concentrations of OH and O$_3$ (especially over the ocean) and uncertainties concerning Hg chemical speciation in emission inventories. The simulated tropospheric mean OH concentration is 1.41×10^6 molec cm^{-3}. This is at the high end of the concentration range (0.65–1.56×10^6 molec cm^{-3}) summarized by Lawrence et al. (2001) and is about 27 % higher than the ensemble mean ($11.1 \pm 1.8 \times 10^5$ molec cm^{-3}) of the Atmospheric Chemistry and Climate Model Intercomparison Project (ACCMIP) models (Voulgarakis et al., 2013). The simulated mean surface O$_3$ in the North Pacific and North Atlantic is overestimated by 27 and 34 % compared to observations from the WDCGG (World Data Centre for Greenhouse Gases) network, although concentrations over land are reproduced relatively well (see Figs. S10 and S11 in the Supplement). Moreover, uncertainties of Hg chemistry (e.g., gas-particle partitioning of RGM, in-plume reduction of RGM) and deposition processes in the present model might also contribute to this discrepancy. Overall, the simulated oxi-

dized mercury concentrations agree with observations within a factor of 5 (Fig. 10). The statistical indicators R and NMB, calculated from 26 land sites, are 0.53 and 3 % (Table 3), respectively.

3.5 Wet deposition

Wet deposition is mainly determined by the distribution of precipitation and Hg concentrations. Figures 6 and 7 evaluate the simulated annual Hg wet deposition and accumulated precipitation over North America, Europe and East Asia. In general, GNAQPMS-Hg reproduces the spatial patterns of Hg wet deposition relatively well.

Over North America, the maximum wet deposition occurs in the southeast, corresponding to high OH concentrations and frequent precipitation there, while less wet deposition occurs in the west and north, where there is much less precipitation. GNAQPMS-Hg predicts the magnitude of mean wet deposition within 5 % and shows a good spatial correlation ($R = 0.76$) (Table 3). These results are similar to those of GEOS-Chem (Selin et al., 2007). However, it should be also noted that precipitation in the southeast is slightly overestimated by the model.

Over Europe, model performance for wet deposition and precipitation are better than over North America and East Asia. High spatial correlation between the simulated and observed results are found for both wet deposition ($R = 0.78$) and precipitation ($R = 0.86$), and the NMBs are both less than 5 % (Table 3).

Over East Asia, Hg wet deposition is not only related to the precipitation pattern but also the local Hg emissions, especially in southwestern China, in the Jilin province of China, and in central Japan. Model performance for wet

Table 3. Statistical summary of comparisons of the model results with observations[a].

Parameter	Region	R	NMB	RMSE	SVR[b]
	East Asia nested	0.51	−39 %	3.87	2.56
	East Asia	0.54	−32 %	3.61	2.56
TGM	North America	0.69	18 %	0.58	0.48
	Europe	0.57	−8 %	0.17	0.35
	Global	0.70	−18 %	2.22	–
	East Asia nested	0.45	−12 %	242	3.66
	East Asia	0.31	−10 %	259	3.66
Oxidized mercury	North America	0.53	148 %	28	1.61
	Europe	0.91	155 %	48	1.00
	Global	0.53	3 %	185	–
	East Asia nested	0.78	−28 %	45.5	6.69
	East Asia	0.36	−61 %	60.1	6.69
Wet deposition	North America	0.76	−4 %	4.3	1.89
	Europe	0.78	4 %	1.5	1.40
	Global	0.38	−36 %	29.3	–
Dry deposition	East Asia nested	0.88	−42 %	87.0	–
	East Asia	0.81	−42 %	88.5	–

[a] R, NMB, RMSE, and SVR represent correlation coefficient, normalized mean bias, root mean square error, and spatial variation ratio. Units of TGM, oxidized mercury, wet and dry deposition are $\mathrm{ng\,m^{-3}}$, $\mathrm{pg\,m^{-3}}$, $\mathrm{\mu g\,m^{-2}\,yr^{-1}}$, $\mathrm{\mu g\,m^{-2}\,yr^{-1}}$, respectively. [b] SVR is defined as $(\mathrm{max}-\mathrm{min})/\mathrm{mean}$ observations over all sites.
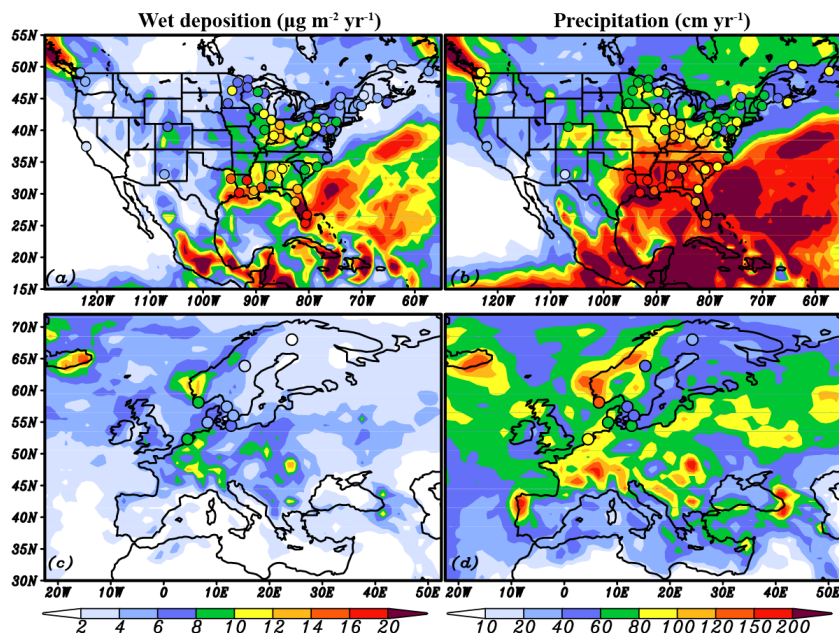
Figure 6. Simulated annual mercury wet deposition ($\mathrm{\mu g\,m^{-2}\,yr^{-1}}$) and accumulated precipitation ($\mathrm{cm\,yr^{-1}}$) over North America **(a, b)** and Europe **(c, d)** in 2001. Overlaid points show observations for the same year from the Mercury Deposition Network (MDN) over North America, and the European Monitoring and Evaluation Programme (EMEP) over Europe.

deposition over East Asia is poorer than over Europe and North America. Although the spatial distribution and magnitude of precipitation over East Asia are seemingly well reproduced ($R = 0.64$ and $\mathrm{NMB} = -6\,\%$), a large underes-

timation ($\mathrm{NMB} = -61\,\%$) of wet deposition is found here. Specifically, this is because the model fails to capture the high wet deposition at certain sites. For example, the observed wet deposition over Shanghai and Changchun are 251
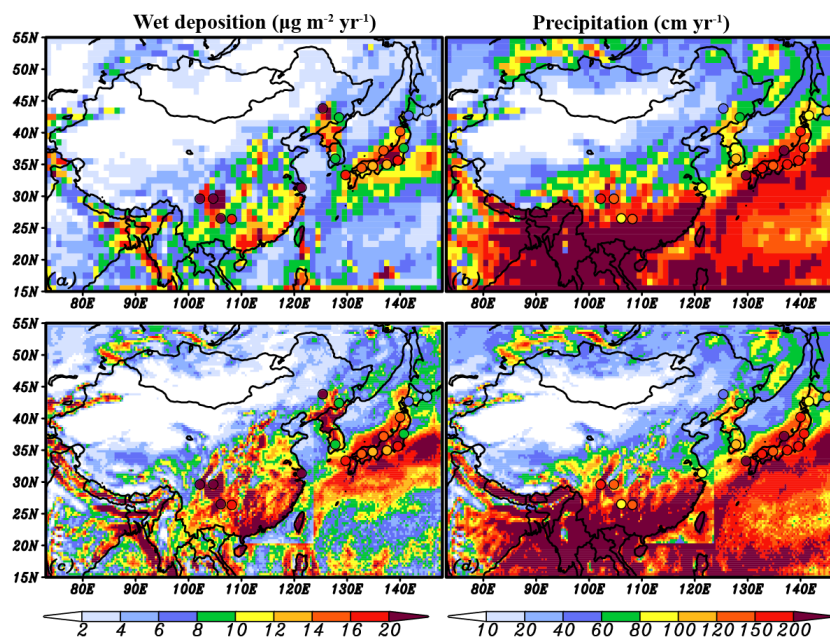
Figure 7. Simulated annual mercury wet deposition (μg m^{-2} yr^{-1}) and accumulated precipitation (cm yr^{-1}) over East Asia in the global **(a, b)** and nested **(c, d)** domains in 2001. Overlaid points show observations collected from the literature. Note that observations and simulated results are not in the same year
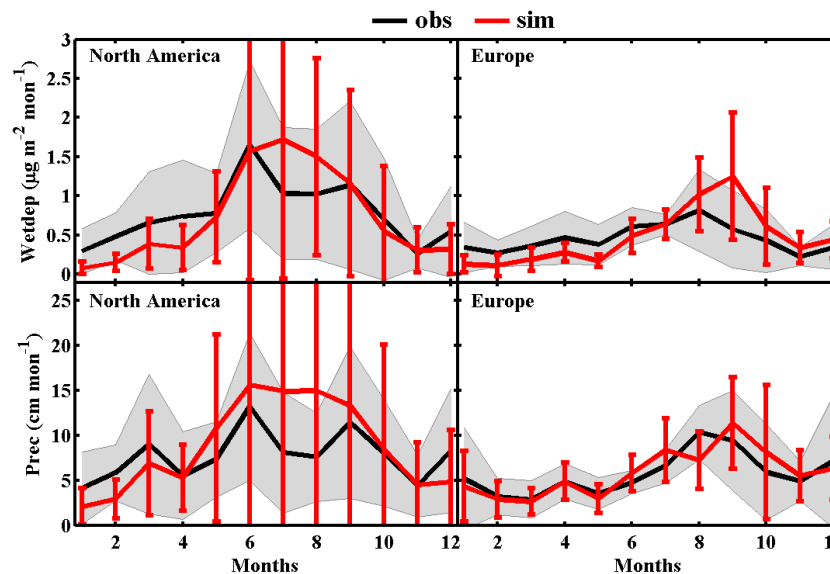

Figure 8. Mean seasonal variation of mercury wet deposition (μg m^{-2} mon^{-1}) and accumulated precipitation (cm mon^{-1}) at North America (51 sites averaged) and Europe (8 sites averaged) sites in 2001. Gray shaded areas and red vertical bars show 1 standard deviation over the sites for observations and for model results.

and 108 μg m^{-2} yr^{-1} while the corresponding simulated values are only 25 and 13 μg m^{-2} yr^{-1}. This suggests that it is hard for models with coarse horizontal resolution to characterize the high local mercury pollution in China. The difference between the simulated and observed time periods and uncertainties in the emission inventories may also contribute to these discrepancies.

Figure 8 further compares the simulated seasonal cycle of wet deposition with measurements at MDN sites over North America and EMEP sites over Europe. No monthly wet deposition observations are available over East Asia. Wet deposition and precipitation share similar monthly variations, with high values in summer and autumn and low values in winter, as shown by both observations and simula-

tion. In summer and autumn, the variation in wet deposition and precipitation among sites is larger than for other seasons, and this is evident from the greater variability in Fig. 8. GNAQPMS-Hg tends to overestimate wet deposition and precipitation in July and August over North America.

3.6 Dry deposition

Due to limited observations, only Hg dry deposition over East Asia is evaluated in this study. It should be noted that data (Table S5 in the Supplement) used to evaluate the model simulation of dry deposition is not directly measured but is inferred or estimated based on measurements of total Hg in throughfall and rainwater, wet deposition and atmospheric concentrations. Associated with local Hg emissions, high dry deposition mainly occurs over central eastern China and central Japan (Fig. 9). The modeled dry deposition has a good spatial correlation with observations ($r = 0.81$), but there is a substantial negative bias (NMB $= -42$ %, Table 3). In general, the simulated dry deposition agrees with observations within a factor of 5 (Fig. 10). Over Japan, the model results are biased high by a factor of 2–5, which may be caused by overestimation of Hg(II) and Hg(P) emissions and a missing model mechanism to deal with fast in-plume reduction of Hg(II) (Vijayaraghavan et al., 2008; Amos et al., 2012; Zhang et al., 2012). Taking Tokyo as an example, observed Hg(P) is only 98 pg m^{-3} while the simulated value is as high as 648 pg m^{-3}. Modeling studies conducted by Pan et al. (2008) using the STEM-Hg model also found large overestimation of dry deposition over Japan. Conversely, the model results are biased low by a factor of 2–5 over China, which indicates probable underestimation of Chinese Hg emissions.

3.7 Model performance summary and comparison

In this section, we summarize the statistical performance of GNAQPMS-Hg for TGM, oxidized mercury, and wet and dry deposition, compare the model performance over East Asia, North America and Europe, and assess the effects of horizontal resolution on model predictions over East Asia. As shown in Fig. 10, the simulated TGM and wet deposition are within a factor of 2 of the corresponding observations and within a factor of 5 for oxidized mercury and dry deposition. The statistical performance of GNAQPMS-Hg is comparable with that of other state-of-the-art Hg models (Bullock et al., 2008; Ryaboshapko et al., 2007; Pirrone and Keating, 2010).

3.7.1 East Asia versus North America and Europe

As illustrated in Table 3, the model statistical performance for all Hg parameters in North America and Europe is better than in East Asia. For example, the RMSEs between simulated and observed TGM over North America and Europe are 0.58 and 0.17 ng m^{-3} but up to 3.61 ng m^{-3} over East Asia. The poor model performance over East Asia is prob-

ably caused by the following reasons. Firstly, there are differences between simulated and observed data periods. Hg measurements over East Asia (especially China) are mainly taken from recent years, and the observed values are higher than in year 2001, which may lead to model underestimation. For example, anthropogenic Hg emissions in China increased by 164 % between 1992 and 2007 (Liang et al., 2013). Secondly, there is a much higher spatial variation ratio (SVR, see Table 3) for Hg parameters in East Asia than in North America and Europe. This implies that there are very intense spatial variations in surface Hg concentrations and deposition over East Asia which cannot be resolved at the coarse horizontal resolution used in global models (see Sect. 3.7.2). Thirdly, there are large uncertainties in emission inventories over East Asia. Large underestimations in anthropogenic Hg emissions over East Asia have been demonstrated in several previous studies (Jaffe et al., 2005; Pan et al., 2007; Friedli et al., 2004; Song et al., 2015). This is consistent with the simulated results in this study. Except for the above factors, missing some chemical and physical processes (e.g., gas-particle partitioning of Hg(II), in-plume reduction of Hg(II), and dynamic land re-emission) in the present model might also contribute to the poor model performance over East Asia.

3.7.2 Global versus nested simulations

In order to assess the impact of resolution on model predictions, an online nested simulation with higher resolution ($0.33° \times 0.33°$) over East Asia was conducted and compared to the global simulation with lower resolution ($1° \times 1°$). Emissions, meteorology, deposition and chemistry are self-consistent between the global and nested domains. The nested simulation uses higher resolution model inputs (e.g., topography, meteorology, emissions) and thus has the potential to better resolve high spatial variability of Hg concentrations and deposition in regional and local scales.

Figures 7 and 9 compare the spatial distributions of simulated annual mercury wet deposition, accumulated precipitation and dry deposition over East Asia between the global and nested simulations. Although the global and nested simulations predict similar large-scale patterns for Hg deposition, the nested simulation resolves many fine features which are lost in the global simulation by horizontal averaging. Firstly, in the nested domain, high-deposition fluxes become more concentrated in regions with large emissions or precipitation resulting in higher spatial variability in deposition. Secondly, the nested simulation reveals elevated wet deposition in southwestern China due to frequent orographic and convective precipitation. Finally, the nested simulation shows a more detailed land/ocean contrast in deposition over coastal regions. For example, over the coastal regions of southeastern China and Japan, wet deposition increases due to scavenging of local emissions and enhanced precipitation (Fig. 7) while dry deposition decreases are associated with the lower dry deposition velocity of Hg(0) over land than
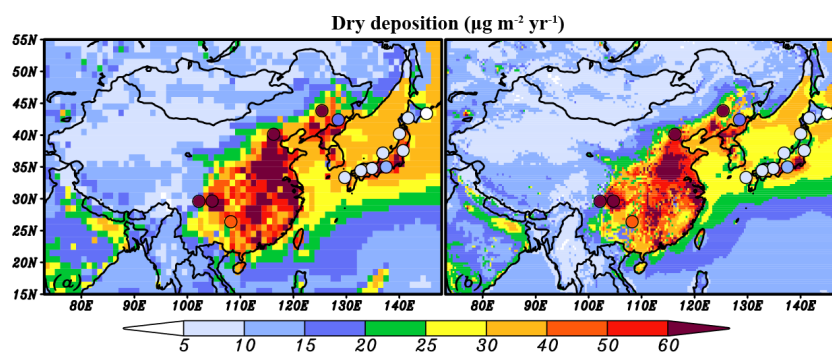
Figure 9. Simulated annual mercury dry deposition ($\mu g\,m^{-2}\,yr^{-1}$) over East Asia in the global **(a)** and nested **(b)** domains in 2001. Overlaid points show observations collected from the literature. Note that observations and simulated results are not in the same year.
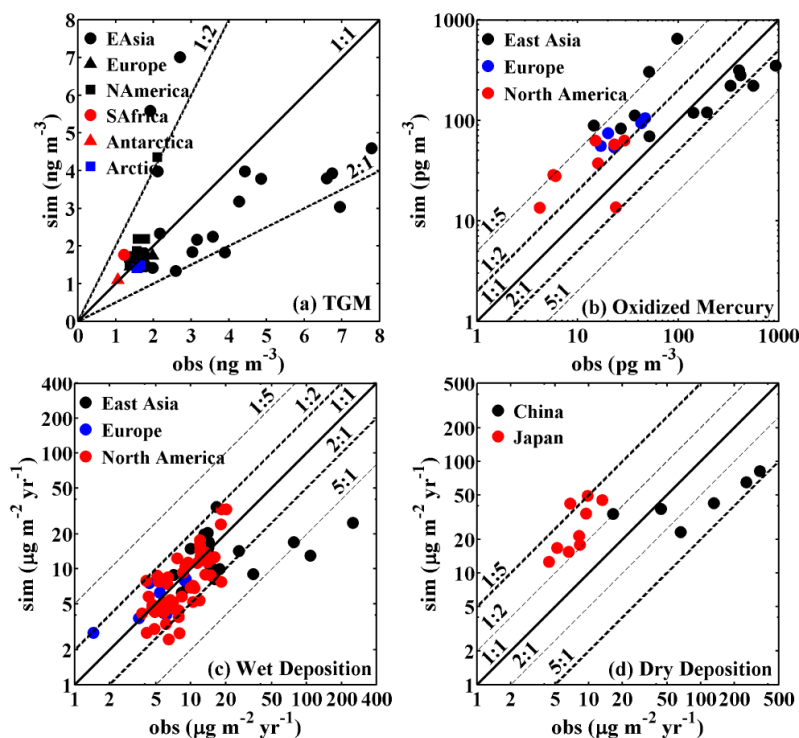

Figure 10. Simulated vs. observed **(a)** TGM ($ng\,m^{-3}$), **(b)** oxidized mercury ($pg\,m^{-3}$), **(c)** wet deposition ($\mu g\,m^{-2}\,yr^{-1}$), **(d)** dry deposition ($\mu g\,m^{-2}\,yr^{-1}$) in different regions. Note that coordinates are different in different panels.

over ocean (Fig. 9). Our results are similar to those of Zhang et al. (2012), who conducted a nested simulation of Hg over North America using the GEOS-Chem model. More comparisons about the differences of dry and wet deposition and Hg budgets over East Asia between the two simulations are given in Fig. S16 and Table S6 in the Supplement.

Figure 11 and Table 3 further quantitatively compare the model performance over East Asia between the global and nested domains. In the Taylor diagram (Taylor, 2001), the position of each circle (or square) quantifies how closely the simulated results match observations. We can see that the simulated precipitation, oxidized Hg, wet and dry depo-

sition agree better with observations in the nested domain than in the global domain (Fig. 11). The largest improvement is found in the simulated wet deposition. Specifically, the statistical parameter R for simulated wet deposition increases from 0.36 to 0.78, the NMB decreases from -61 to -28 %, and the RMSE decreases by 24 % (from 60.1 to 45.5 $\mu g\,m^{-2}\,yr^{-1}$) (Table 3). But for TGM, oxidized Hg and dry deposition, the statistical parameters do not change significantly. For example, the RMSEs of simulated oxidized Hg and dry deposition decrease by 7 and 2 %, respectively, but increase by 7 % for simulated TGM.
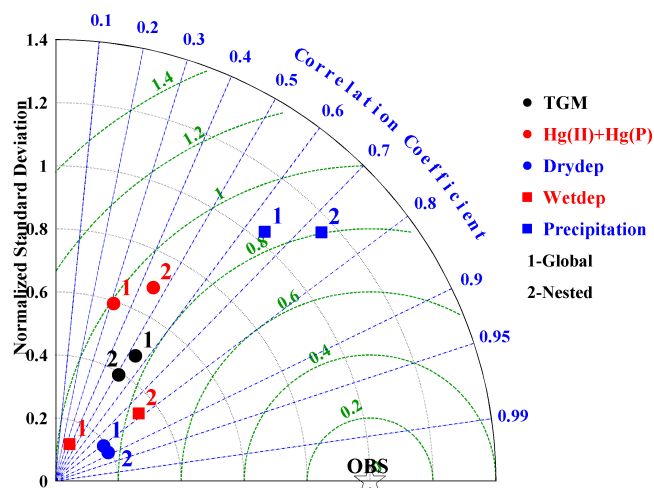
Figure 11. Taylor diagram of simulated annual TGM, Hg(II)+Hg(P), dry deposition, wet deposition and precipitation over East Asia in the global and nested domains (denoted as 1 and 2).

Figure 12. Contributions of Chinese primary anthropogenic sources to (a) annual mercury surface concentrations (ng m^{-3}) and (b) total (wet plus dry) deposition (µg m^{-2} yr^{-1}) in the Northern Hemisphere.

Table 4. Statistical comparisons of the online and offline nested simulation results with observations over East Asia[a].

Parameter	Case[b]	R	NMB	RMSE
TGM	Base simulation	0.51	−39 %	3.87
	3 h boundary conditions	0.50	−42 %	3.94
	6 h boundary conditions	0.50	−42 %	3.95
Oxidized mercury	Base simulation	0.45	−12 %	242.15
	3 h boundary conditions	0.42	−17 %	251.52
	6 h boundary conditions	0.41	−18 %	252.78
Wet deposition	Base simulation	0.78	−28 %	45.47
	3 h boundary conditions	0.78	−29 %	45.75
	6 h boundary conditions	0.78	−29 %	45.78
Dry deposition	Base simulation	0.88	−42 %	87.02
	3 h boundary conditions	0.88	−44 %	88.55
	6 h boundary conditions	0.87	−45 %	88.96

[a] R, NMB, RMSE represent correlation coefficient, normalized mean bias, root mean square error. Units of TGM, oxidized mercury, wet and dry deposition are ng m^{-3}, pg m^{-3}, µg m^{-2} yr^{-1}, µg m^{-2} yr^{-1}, respectively. [b] In the base simulation, the nested domain gets boundary conditions from the global domain every 10 min.

3.7.3   Online versus offline nested simulations

In order to further justify the online nested method, several model sensitivity experiments were conducted and the simulated results were compared to observations over East Asia. In the base simulation, the online nested method was used and the nested domain got boundary conditions from the global domain every 10 min. In the sensitivity simulations, the offline method was used and the boundary conditions were applied at 3 or 6 h. The differences between the base and the sensitivity simulations were mainly caused by different frequency of boundary conditions. As shown in Table 4, the model performances are similar between the two sensitivity simulations (with 3 and 6 h offline boundary con-
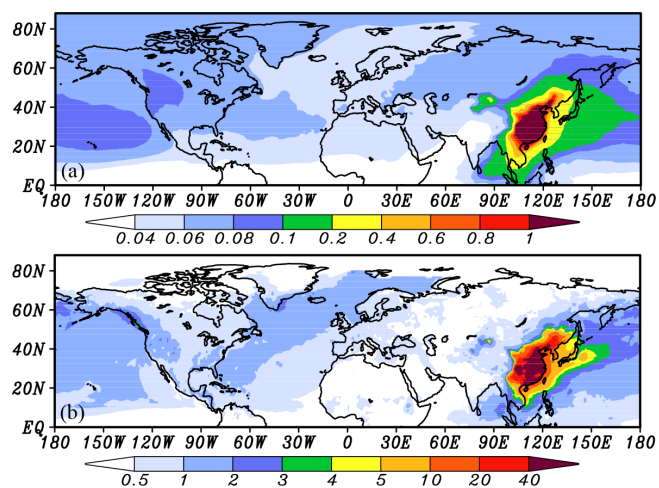
ditions, respectively). While the model performances in the base simulation are slightly better than those in the sensitivity simulations. The largest improvement is found in the simulated oxidized mercury. Specifically, the statistical parameter R for simulated oxidized mercury increases from 0.41 to 0.45, the NMB decreases from −18 to −12 %, and the RMSE decreases by 4 % compared to the simulated results with 6 h offline boundary conditions. For wet deposition, little changes are found. This is because Hg wet deposition is not only affected by air concentrations but also precipitation. These results confirmed the effectiveness of the online nested method.

4   Impacts of Chinese primary anthropogenic sources on global Hg levels

Figure 12 shows the contribution of Chinese primary anthropogenic sources (not including re-emission) to annual mercury surface concentrations and total deposition in the Northern Hemisphere, and Fig. 13 gives the corresponding mean percentage contributions over different world regions (defined in Fig. S17 in the Supplement), as derived from a sensitivity simulation with Chinese anthropogenic emissions shut off. In general, the largest percentage contribution is found in China itself, followed by neighboring regions like the Korean Peninsula, Southeast Asia, Mongolia and Japan, but they are relatively small in other regions. Specifically, domestic anthropogenic emissions contribute on average 0.6 ng m^{-3} (ranging from below 0.1 to above 3.0) to surface Hg concentrations and 18.4 µg m^{-2} yr^{-1} (ranging from below 2.0 to above 50.0) to total deposition in China. They account for about 30 % and 62 % on a national basis, respectively. The domestic contribution to deposition consists mainly of the
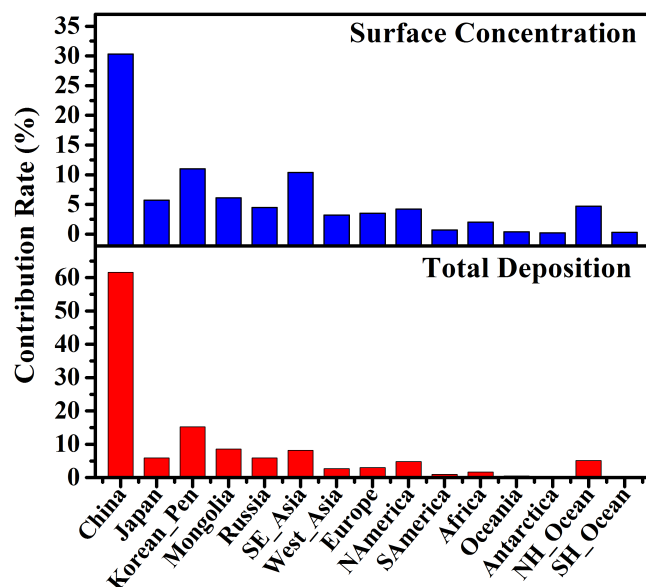
Figure 13. Mean percentage contributions (%) from Chinese primary anthropogenic sources to annual mercury surface concentrations and total (wet plus dry) deposition over different world regions.

deposition of directly emitted Hg(II) and Hg(P) near sources and deposition of Hg(II) formed by oxidation of Chinese Hg(0). For neighboring regions, the Chinese anthropogenic contributions to surface Hg concentrations and deposition are also large. For example, the percentage contributions are 11 % (0.2–$0.6\,\mathrm{ng\,m^{-3}}$) and 15.2 % (8–$20\,\mathrm{\mu g\,m^{-2}\,yr^{-1}}$) over the Korean Peninsula, 10.4 % (0.1–$0.6\,\mathrm{ng\,m^{-3}}$) and 8.2 % (1–$12\,\mathrm{\mu g\,m^{-2}\,yr^{-1}}$) over Southeast Asia, and 5.7 % (0.1–$0.4\,\mathrm{ng\,m^{-3}}$) and 5.9 % (2–$15\,\mathrm{\mu g\,m^{-2}\,yr^{-1}}$) over Japan. For regions far away from China, the percentage contributions are small. They are 4.2 % (0.06–$0.1\,\mathrm{ng\,m^{-3}}$) and 4.8 % (0.5–$4\,\mathrm{\mu g\,m^{-2}\,yr^{-1}}$) over North America and 3.5 % (below $0.08\,\mathrm{ng\,m^{-3}}$) and 3.0 % (below $2.0\,\mathrm{\mu g\,m^{-2}\,yr^{-1}}$) over Europe. The percentage contributions over North America determined from our simulation are comparable with the modeling study of Lei et al. (2013). They estimated that around 7 % of TGM concentrations and 9 % of total Hg deposition in the United States resulted from transpacific transport of Asian anthropogenic emissions. Given that about 53 % of Asian anthropogenic Hg emissions are from China, it is reasonable that our estimated contributions are a little smaller than those reported by Lei et al. (2013).

Finally, there are another two issues which need to be addressed. Firstly, the above analysis mainly focuses on regional average contributions. However, the percentage contributions vary geographically inside the region. As shown in Fig. 12, contributions of domestic anthropogenic emissions to total deposition in central eastern China can exceed $40\,\mathrm{\mu g\,m^{-2}\,yr^{-1}}$, but they are below $5\,\mathrm{\mu g\,m^{-2}\,yr^{-1}}$ in western China. Similarly, previous studies have found that Asian

emissions make a much larger contribution to Hg deposition in the western USA than in the eastern USA (Seigneur et al., 2004; Strode et al., 2008). Secondly, the contributions from re-emission of previously deposited anthropogenic Hg (treated as natural land or ocean re-emission in GNAQPMS-Hg) are not taken into account in this study. Of the natural emissions, only one-third is considered not to be influenced by anthropogenic activities at all (Jung et al., 2009). In addition, according to the modeling study of Selin et al. (2008), 31 % (including 22 % primary and 9 % recycled) of the deposition over the USA is from anthropogenic emissions outside of North America. When considering re-emission of previously deposited anthropogenic Hg, this suggests that the foreign anthropogenic contribution would increase by about 42 % (from 22 to 31 %). If we apply the same scaling factor to our attribution results, then the estimated Chinese anthropogenic contributions to Hg deposition over North America would increase from 4.8 to 6.8 %. Therefore, it is also important to consider the re-emission of previously deposited anthropogenic Hg.

5 Conclusions

A global nested atmospheric mercury transport model including Hg emissions, chemical transformation and deposition is introduced in this study. The treatment of Hg chemistry employs the O_3–OH oxidation and SO_3^{2-}–HO_2 reduction mechanisms. The gas-phase reactions of Hg are added to the CBM-Z mechanism, while the aqueous-phase reactions and wet deposition of Hg are calculated through adapting the RADM mechanism. The Wesely (1989) resistance model is used to deal with Hg dry deposition. The same meteorological fields, emissions, chemical and physical parameterizations are used in the global and nested domains.

The GNAQPMS-Hg model has a global mercury source of $10\,163\,\mathrm{Mg\,yr^{-1}}$, including $2488\,\mathrm{Mg\,yr^{-1}}$ of primary anthropogenic emissions, $675\,\mathrm{Mg\,yr^{-1}}$ of biomass burning emissions, $2000\,\mathrm{Mg\,yr^{-1}}$ of land emissions (of which 75 % is re-emission), and $5000\,\mathrm{Mg\,yr^{-1}}$ from the ocean. Dynamic bidirectional air–surface exchange of Hg is not included in the model. Instead, we simply apply static net emission fluxes to account for natural sources (including re-emission) of Hg, with total emission amounts determined based on published estimates.

Based on existing routine monitoring networks (e.g., MDN, EMEP) and the published literature, global observations including surface Hg concentrations and deposition are collected for model evaluation. Compared with previous studies, many more observations over East Asia (especially China) are included in our data set. Model evaluation shows that the spatial distribution and seasonal cycle of Hg concentrations and deposition can be reproduced reasonably well by GNAQPMS-Hg. Overall, the simulated annual TGM and wet deposition match observations within a factor of 2,

and within a factor of 5 for oxidized mercury and dry deposition. This performance is comparable with other state-of-the-art Hg models. Some model deficiencies have also been identified. GNAQPMS-Hg is systematically biased low relative to cruise observations in the Northern Hemisphere, due to poor representation of the air–sea exchange mechanism for Hg. GNAQPMS-Hg overestimates oxidized mercury concentrations in most parts of the world which may partially be caused by excessive oxidation of Hg(0) by relatively high concentrations of OH and O_3 and uncertainties associated with Hg chemical speciation in emission inventories. The model performs significantly better in North America and Europe than in East Asia. This can probably be attributed to the large uncertainties in emission inventories, coarse model resolution and inconsistency between the simulation and observation periods in East Asia. An online nested simulation with higher resolution ($0.33° \times 0.33°$) over East Asia was conducted to examine the impact of horizontal resolution on model predictions. Relative to the global simulation, the nested simulation can better resolve high spatial variability of Hg concentrations and deposition over East Asia and can better capture features such as higher wet deposition due to orographic and convective precipitation, and land/ocean contrast. Statistically, the RMSE of simulated wet deposition over East Asia is reduced by 24 % in the nested simulation.

To quantify the impacts of Chinese anthropogenic sources on global Hg levels, a model sensitivity simulation was conducted with Chinese anthropogenic emissions shut off. The results show that these sources contribute 30 and 62 % of surface mercury concentrations and deposition over China. Outside of China, the largest percentage contributions of 11 and 15.2 % are found in the Korean Peninsula, followed by Southeast Asia (10.4 and 8.2 %), Mongolia (6.1 and 8.6 %), and Japan (5.7 and 5.9 %). For regions far away from China, the percentage contributions are relatively small (e.g., 4.2 and 4.8 % over North America; 3.5 and 3.0 % over Europe).

To perfect the model, future improvements will be focused on the following aspects: (1) employing dynamic parameterizations for bidirectional air–surface (sea and land) exchange of Hg (Selin et al., 2008; Bash, 2010; Strode et al., 2007) to better reflect natural emissions (including re-emission), (2) including fast in-plume reduction of Hg(II) to better characterize Hg(II) distribution near large point sources (Amos et al., 2012), and (3) reducing uncertainties in the anthropogenic Hg emission inventory, especially the Hg speciation profile. Finally, establishing routine Hg monitoring networks would also be very helpful for enhancing and improving modeling studies in East Asia.

Code availability

Please contact Huansheng Chen (email: chenhuansheng@mail.iap.ac.cn) to obtain the source code of GNAQPMS-Hg.

The Supplement related to this article is available online at doi:10.5194/gmd-8-2857-2015-supplement.

References

AMAP/UNEP: Technical Background Report to the Global Atmospheric Mercury Assessment, Tech. rep., Arctic Monitoring and Assessment Programme/UNEP Chemicals Branch, available at: http://www.unep.org/chemicalsandwaste/Metals/Mercury/Informationmaterials/ReportsandPublications/tabid/3593/Default.aspx (last access: 9 September 2015), 2008.

AMAP/UNEP: Technical Background Report for the Global Mercury Assessment 2013, Tech. rep., Arctic Monitoring and Assessment Programme AMAP and United Nations Environment Programme (UNEP) Chemicals Branch, available at: http://www.unep.org/hazardoussubstances/Mercury/Informationmaterials/ReportsandPublications/tabid/3593/Default.aspx (last access: 9 September 2015), 2013.

Amos, H. M., Jacob, D. J., Holmes, C. D., Fisher, J. A., Wang, Q., Yantosca, R. M., Corbitt, E. S., Galarneau, E., Rutter, A. P., Gustin, M. S., Steffen, A., Schauer, J. J., Graydon, J. A., Louis, V. L. St., Talbot, R. W., Edgerton, E. S., Zhang, Y., and Sunderland, E. M.: Gas-particle partitioning of atmospheric Hg(II) and its effect on global mercury deposition, Atmos. Chem. Phys., 12, 591–603, doi:10.5194/acp-12-591-2012, 2012.

Ariya, P. A., Khalizov, A., and Gidas, A.: Reactions of gaseous mercury with atomic and molecular halogens: Kinetics, product studies, and atmospheric implications, J. Phys. Chem. A, 106, 7310–7320, doi:10.1021/jp020719o, 2002.

Bash, J. O.: Description and initial simulation of a dynamic bidirectional air-surface exchange model for mercury in Community Multiscale Air Quality (CMAQ) model, J. Geophys. Res.-Atmos., 115, D06305, doi:10.1029/2009jd012834, 2010.

Bergan, T. and Rodhe, H.: Oxidation of elemental mercury in the atmosphere: constraints imposed by global scale modelling, J. Atmos. Chem., 40, 191–212, doi:10.1023/a:1011929927896, 2001.

Bullock, O. R. and Brehme, K. A.: Atmospheric mercury simulation using the CMAQ model: formulation description and analysis of wet deposition results, Atmos. Environ., 36, 2135–2146, doi:10.1016/s1352-2310(02)00220-0, 2002.

Bullock Jr., O. R., Atkinson, D., Braverman, T., Civerolo, K., Dastoor, A., Davignon, D., Ku, J.-Y., Lohman, K., Myers, T. C., Park, R. J., Seigneur, C., Selin, N. E., Sistla, G., and Vijayaraghavan, K.: The North American Mercury Model Inter-

comparison Study (NAMMIS): Study description and model-to-model comparisons, J. Geophys. Res.-Atmos., 113, D17310, doi:10.1029/2008jd009803, 2008.

Chang, J. S., Brost, R. A., Isaksen, I. S. A., Madronich, S., Middleton, P., Stockwell, W. R., and Walcek, C. J.: A three-dimensional Eulerian acid deposition model: Physical concepts and formulation, J. Geophys. Res.-Atmos., 92, 14681–14700, doi:10.1029/JD092iD12p14681, 1987.

Christensen, J. H., Brandt, J., Frohn, L. M., and Skov, H.: Modelling of Mercury in the Arctic with the Danish Eulerian Hemispheric Model, Atmos. Chem. Phys., 4, 2251–2257, doi:10.5194/acp-4-2251-2004, 2004.

Clever, H. L., Johnson, S. A., and Derrick, M. E.: The solubility of mercury and some sparingly soluble mercury salts in water and aqueous-electrolyte solutions, J. Phys. Chem. Ref. Data, 14, 631–681, 1985.

Corbitt, E. S., Jacob, D. J., Holmes, C. D., Streets, D. G., and Sunderland, E. M.: Global source-receptor relationships for mercury deposition under present-day and 2050 emissions scenarios, Environ. Sci. Technol., 45, 10477–10484, doi:10.1021/es202496y, 2011.

Dastoor, A. P. and Durnford, D. A.: Arctic Ocean: Is It a Sink or a Source of Atmospheric Mercury, Environ. Sci. Technol., 48, 1707–1717, 2014.

De Simone, F., Gencarelli, C. N., Hedgecok, I. M., and Pirrone, N.: Global atmospheric cycle of mercury: a model study on the impact of oxidation mechanisms, Environ. Sci. Pollut. Res., 21, 4110–4123, 2014.

ENVIRON: User's guide for Comprehensive Air Quality Model with Extensions Version 5.40, ENVIRON International Corporation, Novato, California, 2011.

Frank, D. G.: Mineral Resource Data System (MRDS) data in Arc-View shape file format, for spatial data delivery project, U.S. Geol. Surv., Spokane, Wash., 1999.

Friedli, H. R., Radke, L. F., Prescott, R., Li, P., Woo, J. H., and Carmichael, G. R.: Mercury in the atmosphere around Japan, Korea, and China as observed during the 2001 ACE-Asia field campaign: Measurements, distributions, sources, and implications, J. Geophys. Res.-Atmos., 109, D19s25, doi:10.1029/2003jd004244, 2004.

Friedli, H. R., Arellano, A. F., Cinnirella, S., and Pirrone, N.: Initial estimates of mercury emissions to the atmosphere from global biomass burning, Environ. Sci. Technol., 43, 3507–3513, doi:10.1021/es802703g, 2009.

Fu, X., Feng, X., Sommar, J., and Wang, S.: A review of studies on atmospheric mercury in China, Sci. Total Environ., 421, 73–81, doi:10.1016/j.scitotenv.2011.09.089, 2012.

Ge, B., Wang, Z., Xu, X., Wu, J., Yu, X., and Li, J.: Wet deposition of acidifying substances in different regions of China and the rest of East Asia: Modeling with updated NAQPMS, Environ. Pollut., 187, 10–21, doi:10.1016/j.envpol.2013.12.014, 2014.

Gencarelli, C. N., De Simone, F., Hedgecok, I. M., Sprovieri, F., and Pirrone, N.: Development and application of a regional-scale atmospheric mercury model based on WRF/Chem: a Mediterranean area investigation, Environ. Sci. Pollut. Res., 21, 4095–4109, 2014.

Granier, C., Lamarque, J. F., Mieville, A., Muller, J. F., and Olivier, J.: POET, a database of surface emissions of ozone precursors, tech. report, available at: http://www.aero.jussieu.fr/projet/ACCENT/POET.php (last access: 10 June 2013), 2005.

Guenther, A., Karl, T., Harley, P., Wiedinmyer, C., Palmer, P. I., and Geron, C.: Estimates of global terrestrial isoprene emissions using MEGAN (Model of Emissions of Gases and Aerosols from Nature), Atmos. Chem. Phys., 6, 3181–3210, doi:10.5194/acp-6-3181-2006, 2006.

Hall, B.: The gas phase oxidation of elemental mercury by ozone, Water Air Soil Pollut., 80, 301–315, doi:10.1007/bf01189680, 1995.

Hall, B. and Bloom., N.: Report to EPRI, Palo Alto, CA., USA, 1993.

Harada, M.: Minamata Disease – Methylmercury poisoning in Japan caused by environmental pollution, Crit. Rev. Toxicol., 25, 1–24, doi:10.3109/10408449509089885, 1995.

Holmes, C. D., Jacob, D. J., Corbitt, E. S., Mao, J., Yang, X., Talbot, R., and Slemr, F.: Global atmospheric model for mercury including oxidation by bromine atoms, Atmos. Chem. Phys., 10, 12037–12057, doi:10.5194/acp-10-12037-2010, 2010.

Horowitz, L. W., Walters, S., Mauzerall, D. L., Emmons, L. K., Rasch, P. J., Granier, C., Tie, X. X., Lamarque, J. F., Schultz, M. G., Tyndall, G. S., Orlando, J. J., and Brasseur, G. P.: A global simulation of tropospheric ozone and related tracers: Description and evaluation of MOZART, version 2, J. Geophys. Res.-Atmos., 108, 4784, doi:10.1029/2002jd002853, 2003.

Jaffe, D. and Strode, S.: Sources, fate and transport of atmospheric mercury from Asia, Environ. Chem., 5, 121–126, doi:10.1071/en08010, 2008.

Jaffe, D., Prestbo, E., Swartzendruber, P., Weiss-Penzias, P., Kato, S., Takami, A., Hatakeyama, S., and Kajii, Y.: Export of atmospheric mercury from Asia, Atmos. Environ., 39, 3029–3038, doi:10.1016/j.atmosenv.2005.01.030, 2005.

Jiang, G., Shi, J., and Feng, X.: Mercury pollution in China: An overview of the past and current sources of the toxic metal, Environ. Sci. Technol., 40, 3673–3678, 2006.

Jung, G., Hedgecock, I. M., and Pirrone, N.: ECHMERIT V1.0 – a new global fully coupled mercury-chemistry and transport model, Geosci. Model Dev., 2, 175–195, doi:10.5194/gmd-2-175-2009, 2009.

Keeler, G. J., Pirrone, N., Bullock, R., and Sillman, S.: The need for a coordinated global Hg monitoring network for global and regional models validation, in: Mercury Fate and Transport in the Global Atmosphere, edited by: Mason, R., and Pirrone, N., Springer, USA, 391-424, 2009.

Lamarque, J.-F., Bond, T. C., Eyring, V., Granier, C., Heil, A., Klimont, Z., Lee, D., Liousse, C., Mieville, A., Owen, B., Schultz, M. G., Shindell, D., Smith, S. J., Stehfest, E., Van Aardenne, J., Cooper, O. R., Kainuma, M., Mahowald, N., McConnell, J. R., Naik, V., Riahi, K., and van Vuuren, D. P.: Historical (1850–2000) gridded anthropogenic and biomass burning emissions of reactive gases and aerosols: methodology and application, Atmos. Chem. Phys., 10, 7017–7039, doi:10.5194/acp-10-7017-2010, 2010.

Lamborg, C. H., Fitzgerald, W. F., O'Donnell, J., and Torgersen, T.: A non-steady-state compartmental model of global-scale mercury biogeochemistry with interhemispheric atmospheric gradients, Geochim. Cosmochim. Ac., 66, 1105-1118, doi:10.1016/s0016-7037(01)00841-9, 2002.

Lawrence, M. G., Jöckel, P., and von Kuhlmann, R.: What does the global mean OH concentration tell us?, Atmos. Chem. Phys., 1, 37–49, doi:10.5194/acp-1-37-2001, 2001.

Lei, H., Liang, X.-Z., Wuebbles, D. J., and Tao, Z.: Model analyses of atmospheric mercury: present air quality and effects of transpacific transport on the United States, Atmos. Chem. Phys., 13, 10807–10825, doi:10.5194/acp-13-10807-2013, 2013.

Li, J., Wang, Z., Akimoto, H., Gao, C., Pochanart, P., and Wang, X.: Modeling study of ozone seasonal cycle in lower troposphere over east Asia, J. Geophys. Res.-Atmos., 112, D22s25, doi:10.1029/2006jd008209, 2007.

Li, J., Wang, Z., Wang, X., Yamaji, K., Takigawa, M., Kanaya, Y., Pochanart, P., Liu, Y., Irie, H., Hu, B., Tanimoto, H., and Akimoto, H.: Impacts of aerosols on summertime tropospheric photolysis frequencies and photochemistry over Central Eastern China, Atmos. Environ., 45, 1817–1829, doi:10.1016/j.atmosenv.2011.01.016, 2011.

Li, J., Wang, Z., Zhuang, G., Luo, G., Sun, Y., and Wang, Q.: Mixing of Asian mineral dust with anthropogenic pollutants over East Asia: a model case study of a super-duststorm in March 2010, Atmos. Chem. Phys., 12, 7591–7607, doi:10.5194/acp-12-7591-2012, 2012.

Liang, S., Xu, M., Liu, Z., Suh, S. and Zhang T.: Socioeconomic Drivers of Mercury Emissions in China from 1992 to 2007, Environ. Sci. Technol., 47, 3234–3240, 2013.

Lin, C. J. and Pehkonen, S. O.: Aqueous free radical chemistry of mercury in the presence of iron oxides and ambient aerosol, Atmos. Environ., 31, 4125–4137, doi:10.1016/S1352-2310(97)00269-0, 1997.

Lin, C. J. and Pehkonen, S. O.: Oxidation of elemental mercury by aqueous chlorine (HOCl/OCl$^-$): Implications for tropospheric mercury chemistry, J. Geophys. Res.-Atmos., 103, 28093–28102, doi:10.1029/98jd02304, 1998.

Lin, C. J. and Pehkonen, S. O.: The chemistry of atmospheric mercury: a review, Atmos. Environ., 33, 2067–2079, doi:10.1016/s1352-2310(98)00387-2, 1999.

Lin, C. J., Pongprueks, P., Ho, T. C., and Jang, C.: Development of mercury modeling schemes within CMAQ framework: Science and model implementation issues, In: Proceedings of the 2004 CMAS Models-3 Conference, Research Triangle Park, NC, 18–20 October (CD-ROM), 2004.

Lin, C. J., Pongprueksa, P., Lindberg, S. E., Pehkonen, S. O., Byun, D., and Jang, C.: Scientific uncertainties in atmospheric mercury models I: Model science evaluation, Atmos. Environ., 40, 2911–2928, doi:10.1016/j.atmosenv.2006.01.009, 2006.

Lindberg, S., Bullock, R., Ebinghaus, R., Engstrom, D., Feng, X., Fitzgerald, W., Pirrone, N., Prestbo, E., and Seigneur, C.: A synthesis of progress and uncertainties in attributing the sources of mercury in deposition, Ambio, 36, 19–32, 2007.

Lindqvist, O. and Rodhe, H.: Atmospheric mercury – A review, Tellus B, 37, 136–159, 1985.

Mason, R.: Mercury emissions from natural processes and their importance in the global mercury cycle, in: Mercury Fate and Transport in the Global Atmosphere, edited by: Mason, R. and Pirrone, N., Springer, USA, 173–191, 2009.

Munthe, J.: The aqueous oxidation of elemental mercury by ozone, Atmos. Environ., 26, 1461–1468, doi:10.1016/0960-1686(92)90131-4, 1992.

Pacyna, E. G., Pacyna, J. M., Steenhuisen, F., and Wilson, S.: Global anthropogenic mercury emission inventory for 2000, Atmos. Environ., 40, 4048–4063, doi:10.1016/j.atmosenv.2006.03.041, 2006.

Pan, L., Chai, T., Carmichael, G. R., Tang, Y., Streets, D., Woo, J.-H., Friedli, H. R., and Radke, L. F.: Top-down estimate of mercury emissions in China using four-dimensional variational data assimilation, Atmos. Environ., 41, 2804–2819, doi:10.1016/j.atmosenv.2006.11.048, 2007.

Pan, L., Carmichael, G. R., Adhikary, B., Tang, Y., Streets, D., Woo, J.-H., Friedli, H. R., and Radke, L. F.: A regional analysis of the fate and transport of mercury in East Asia and an assessment of major uncertainties, Atmos. Environ., 42, 1144–1159, doi:10.1016/j.atmosenv.2007.10.045, 2008.

Pehkonen, S. O. and Lin, C. J.: Aqueous photochemistry of mercury with organic acids, J. Air Waste Manage. Assoc., 48, 144–150, doi:10.1080/10473289.1998.10463661, 1998.

Pirrone, N. and Keating, T.: Hemispheric Transport of Air Pollution 2010 Part B: Mercury, United Nations, New York and Geneva, 210 pp., 2010.

Pirrone, N., Cinnirella, S., Feng, X., Finkelman, R. B., Friedli, H. R., Leaner, J., Mason, R., Mukherjee, A. B., Stracher, G. B., Streets, D. G., and Telmer, K.: Global mercury emissions to the atmosphere from anthropogenic and natural sources, Atmos. Chem. Phys., 10, 5951–5964, doi:10.5194/acp-10-5951-2010, 2010.

Price, C., Penner, J., and Prather, M.: NO$_x$ from lightning: 1. Global distribution based on lightning physics, J. Geophys. Res.-Atmos., 102, 5929–5941, doi:10.1029/96jd03504, 1997.

Ryaboshapko, A., Bullock, O. R., Jr., Christensen, J., Cohen, M., Dastoor, A., Ilyin, I., Petersen, G., Syrakov, D., Travnikov, O., Artz, R. S., Davignon, D., Draxler, R. R., Munthe, J., and Pacyna, J.: Intercomparison study of atmospheric mercury models: 2. Modelling results vs. long-term observations and comparison of country deposition budgets, Sci. Total Environ., 377, 319–333, doi:10.1016/j.scitotenv.2007.01.071, 2007.

Sanemasa, I.: The solubility of elemental mercury vapor in water, Bull. Chem. Soc. Jpn., 48, 1795–1798, 1975.

Schroeder, W. H. and Munthe, J.: Atmospheric mercury – An overview, Atmos. Environ., 32, 809–822, doi:10.1016/s1352-2310(97)00293-8, 1998.

Schroeder, W. H., Anlauf, K. G., Barrie, L. A., Lu, J. Y., Steffen, A., Schneeberger, D. R., and Berg, T.: Arctic springtime depletion of mercury, Nature, 394, 331–332, doi:10.1038/28530, 1998.

Seigneur, C., Abeck, H., Chia, G., Reinhard, M., Bloom, N. S., Prestbo, E., and Saxena, P.: Mercury adsorption to elemental carbon (soot) particles and atmospheric particulate matter, Atmos. Environ., 32, 2649–2657, doi:10.1016/S1352-2310(97)00415-9, 1998.

Seigneur, C., Karamchandani, P., Lohman, K., Vijayaraghavan, K., and Shia, R. L.: Multiscale modeling of the atmospheric fate and transport of mercury, J. Geophys. Res.-Atmos., 106, 27795–27809, doi:10.1029/2000jd000273, 2001.

Seigneur, C., Vijayaraghavan, K., Lohman, K., Karamchandani, P., and Scott, C.: Global source attribution for mercury deposition in the United States, Environ. Sci. Technol., 38, 555–569, doi:10.1021/es034109t, 2004.

Selin, N. E.: Global biogeochemical cycling of mercury: A review, Annu. Rev. Environ. Resour., 34, 43–63, doi:10.1146/annurev.environ.051308.084314, 2009.

Selin, N. E., Jacob, D. J., Park, R. J., Yantosca, R. M., Strode, S., Jaegle, L., and Jaffe, D.: Chemical cycling and deposition of atmospheric mercury: Global constraints from observations, J. Geophys. Res.-Atmos., 112, D02308, doi:10.1029/2006jd007450, 2007.

Selin, N. E., Jacob, D. J., Yantosca, R. M., Strode, S., Jaegle, L., and Sunderland, E. M.: Global 3-D land-ocean-atmosphere model for mercury: Present-day versus preindustrial cycles and anthropogenic enrichment factors for deposition, Global Biogeochem. Cy., 22, Gb3099, doi:10.1029/2008gb003282, 2008.

Shia, R. L., Seigneur, C., Pai, P., Ko, M., and Dak Sze, N.: Global simulation of atmospheric mercury concentrations and deposition fluxes, J. Geophys. Res.-Atmos., 104, 23747–23760, 1999.

Sillen, L. G., Martell, A. E., and Bjerrum, J.: Stability constants of metal-ion complexes, Chem. Soc., 17, 754 pp., 1964.

Soerensen, A. L., Skov, H., Jacob, D. J., Soerensen, B. T., and Johnson, M. S.: Global concentrations of gaseous elemental mercury and reactive gaseous mercury in the marine boundary layer, Environ. Sci. Technol., 44, 7425–7430, doi:10.1021/es903839n, 2010a.

Soerensen, A. L., Sunderland, E. M., Holmes, C. D., Jacob, D. J., Yantosca, R. M., Skov, H., Christensen, J. H., Strode, S. A., and Mason, R. P.: An improved global model for air-sea exchange of mercury: High concentrations over the North Atlantic, Environ. Sci. Technol., 44, 8574–8580, doi:10.1021/es102032g, 2010b.

Soerensen, A. L., Jacob, D. J., Streets, D., Witt, M., Ebinghaus, R., Mason, R. P., Andersson, M., and Sunderland, E. M.: Multidecadal decline of mercury in the North Atlantic atmosphere explained by changing subsurface seawater concentrations, Geophys. Res. Lett., 39, L21810, doi:10.1029/2012GL053736, 2012.

Sommar, J., Gardfeldt, K., Stromberg, D., and Feng, X. B.: A kinetic study of the gas-phase reaction between the hydroxyl radical and atomic mercury, Atmos. Environ., 35, 3049–3054, doi:10.1016/s1352-2310(01)00108-x, 2001.

Song, S., Selin, N. E., Soerensen, A. L., Angot, H., Artz, R., Brooks, S., Brunke, E.-G., Conley, G., Dommergue, A., Ebinghaus, R., Holsen, T. M., Jaffe, D. A., Kang, S., Kelley, P., Luke, W. T., Magand, O., Marumoto, K., Pfaffhuber, K. A., Ren, X., Sheu, G.-R., Slemr, F., Warneke, T., Weigelt, A., Weiss-Penzias, P., Wip, D. C., and Zhang, Q.: Top-down constraints on atmospheric mercury emissions and implications for global biogeochemical cycling, Atmos. Chem. Phys., 15, 7103–7125, doi:10.5194/acp-15-7103-2015, 2015.

Sprovieri, F., Pirrone, N., Ebinghaus, R., Kock, H., and Dommergue, A.: A review of worldwide atmospheric mercury measurements, Atmos. Chem. Phys., 10, 8245–8265, doi:10.5194/acp-10-8245-2010, 2010.

Steffen, A., Schroeder, W., Macdonald, R., Poissant, L., and Konoplev, A.: Mercury in the Arctic atmosphere: An analysis of eight years of measurements of GEM at Alert (Canada) and a comparison with observations at Amderma (Russia) and Kuujjuarapik (Canada), Sci. Total Environ., 342, 185–198, doi:10.1016/j.scitotenv.2004.12.048, 2005.

Strode, S. A., Jaegle, L., Selin, N. E., Jacob, D. J., Park, R. J., Yantosca, R. M., Mason, R. P., and Slemr, F.: Air-sea exchange in the global mercury cycle, Global Biogeochem. Cy., 21, Gb1017, doi:10.1029/2006gb002766, 2007.

Strode, S. A., Jaegle, L., Jaffe, D. A., Swartzendruber, P. C., Selin, N. E., Holmes, C., and Yantosca, R. M.: Trans-Pacific transport of mercury, J. Geophys. Res.-Atmos., 113, D15305, doi:10.1029/2007jd009428, 2008.

Tang, X., Wang, Z., Zhu, J., Gbaguidi, A. E., Wu, Q., Li, J., and Zhu, T.: Sensitivity of ozone to precursor emissions in urban Beijing with a Monte Carlo scheme, Atmos. Environ., 44, 3833–3842, doi:/10.1016/j.atmosenv.2010.06.026, 2010.

Taylor, K. E.: Summarizing multiple aspects of model performance in a single diagram, J. Geophys. Res.-Atmos., 106, 7183–7192, doi:10.1029/2000jd900719, 2001.

Temme, C., Slemr, F., Ebinghaus, R., and Einax, J. W.: Distribution of mercury over the Atlantic Ocean in 1996 and 1999–2001, Atmos. Environ., 37, 1889–1897, doi:10.1016/s1352-2310(03)00069-4, 2003.

Tokos, J. J. S., Hall, B., Calhoun, J. A., and Prestbo, E. M.: Homogeneous gas-phase reaction of $Hg0$ with H_2O_2, O_3, $CH3I$, and $(CH3)(2)S$: Implications for atmospheric Hg cycling, Atmos. Environ., 32, 823–827, doi:10.1016/s1352-2310(97)00171-4, 1998.

Travnikov, O.: Contribution of the intercontinental atmospheric transport to mercury pollution in the Northern Hemisphere, Atmos. Environ., 39, 7541–7548, doi:10.1016/j.atmosenv.2005.07.066, 2005.

Travnikov, O. and Ilyin, I.: The EMEP/MSC-E mercury modeling system, in: Mercury Fate and Transport in the Global Atmosphere, edited by: Mason, R., and Pirrone, N., Springer, USA, 571–587, 2009.

Van Loon, L., Mader, E., and Scott, S. L.: Reduction of the aqueous mercuric ion by sulfite?: UV spectrum of $HgSO_3$ and its intramolecular redox reaction, J. Phys. Chem. A, 104, 1621–1626, doi:10.1021/jp994268s, 2000.

Van Loon, L. L., Mader, E. A., and Scott, S. L.: Sulfite stabilization and reduction of the aqueous mercuric ion: Kinetic determination of sequential formation constants, J. Phys. Chem. A, 105, 3190–3195, doi:10.1021/jp003803h, 2001.

Vijayaraghavan, K., Karamchandani, P., Seigneur, C., Balmori, R., and Chen, S.-Y.: Plume-in-grid modeling of atmospheric mercury, J. Geophys. Res., 113, D24305, doi:10.1029/2008JD010580, 2008.

Voulgarakis, A., Naik, V., Lamarque, J.-F., Shindell, D. T., Young, P. J., Prather, M. J., Wild, O., Field, R. D., Bergmann, D., Cameron-Smith, P., Cionni, I., Collins, W. J., Dalsøren, S. B., Doherty, R. M., Eyring, V., Faluvegi, G., Folberth, G. A., Horowitz, L. W., Josse, B., MacKenzie, I. A., Nagashima, T., Plummer, D. A., Righi, M., Rumbold, S. T., Stevenson, D. S., Strode, S. A., Sudo, K., Szopa, S., and Zeng, G.: Analysis of present day and future OH and methane lifetime in the ACCMIP simulations, Atmos. Chem. Phys., 13, 2563–2587, doi:10.5194/acp-13-2563-2013, 2013.

Walcek, C. J. and Aleksic, N. M.: A simple but accurate mass conservative, peak-preserving, mixing ratio bounded advection algorithm with Fortran code, Atmos. Environ., 32, 3863–3880, doi:10.1016/s1352-2310(98)00099-5, 1998.

Wang, Q., Fu, Q., Wang, Z., Wang, T., Liu, P., Lu, T., Duan, Y., and Huang, Y.: Application of ensemble numerical model system on the air quality forecast in Shanghai, Environ. Monitor. Forewarn., 2, 1–6 + p. 11, 2010 (in Chinese).

Wang, Z., Akimoto, H., and Uno, I.: Neutralization of soil aerosol and its impact on the distribution of acid rain over east Asia: Observations and model results, J. Geophys. Res.-Atmos., 107, 4389, doi:10.1029/2001jd001040, 2002.

Wang, Z., Xie, F., Wang, X., An, J., and Zhu, J.: Development and application of Nested Air Quality Prediction Modeling System, Ch. J. Atmos. Sci., 30, 778–790, 2006 (in Chinese).

Wang, Z., Wu, Q., Gbaguidi, A., Yan, P., Zhang, W., Wang, W., and Tang, X.: Ensemble air quality multi-model forecast system for Beijing (EMS-Beijing): Model description and preliminary application, Journal of Nanjing University of Information Science & Technology (Natural Science Edition), 1, 19–26, 2009 (in Chinese).

Wesely, M. L.: Parameterization of surface resistances to gaseous dry deposition in regional-scale numerical models, Atmos. Environ., 23, 1293–1304, doi:10.1016/0004-6981(89)90153-4, 1989.

Wilson, S. J., Steenhuisen, F., Pacyna, J. M., and Pacyna, E. G.: Mapping the spatial distribution of global anthropogenic mercury atmospheric emission inventories, Atmos. Environ., 40, 4621–4632, doi:10.1016/j.atmosenv.2006.03.042, 2006.

Wu, Q., Wang, Z., Chen, H., Zhou, W., and Wenig, M.: An evaluation of air quality modeling over the Pearl River Delta during November 2006, Meteorol. Atmos. Phys., 116, 113–132, doi:10.1007/s00703-011-0179-z, 2012.

Yan, X., Ohara, T., and Akimoto, H.: Statistical modeling of global soil NOx emissions, Global Biogeochem. Cy., 19, GB3019, doi:10.1029/2004GB002276, 2005.

Zaveri, R. and Peters, L.: A new lumped structure photochemical mechanism for large-scale applications, J. Geophys. Res.-Atmos., 104, 30387–30415, 1999.

Zhang, Y., Jaeglé, L., van Donkelaar, A., Martin, R. V., Holmes, C. D., Amos, H. M., Wang, Q., Talbot, R., Artz, R., Brooks, S., Luke, W., Holsen, T. M., Felton, D., Miller, E. K., Perry, K. D., Schmeltz, D., Steffen, A., Tordon, R., Weiss-Penzias, P., and Zsolway, R.: Nested-grid simulation of mercury over North America, Atmos. Chem. Phys., 12, 6095–6111, doi:10.5194/acp-12-6095-2012, 2012.